CAPITAL UNIVERSITY OF SCIENCE AND TECHNOLOGY, ISLAMABAD

The Extended Mode-Matching Method for a General Impedance Condition in Cylindrical Waveguide

by

Saeed Abbas

A thesis submitted in partial fulfillment for the degree of Master of Philosophy

in the

Faculty of Computing
Department of Mathematics

2025

I dedicate this effort to my Family, my dear Parents, my elegant Teachers and my supervisor Dr. Abdul Rehman Kashif who are always source of inspiration for me and their contributions are uncounted.

CERTIFICATE OF APPROVAL

The Extended Mode-Matching Method for a General Impedance Condition in Cylindrical Waveguide

by

Saeed Abbas

(MMT231014)

THESIS EXAMINING COMMITTEE

(a)	External Examiner	Dr. Muhammad Ayub	QAU, Islamabad
(b)	Internal Examiner	Dr. Rashid Ali	CUST, Islamabad
(c)	Supervisor	Dr. Abdul Rehman Kashif	CUST, Islamabad

Dr. Abdul Rehman Kashif
Thesis Supervisor
August, 2025

Dr. Muhammad Sagheer
Head
Dept. of Mathematics
August, 2025

Dr. Muhammad Abdul Qadir
Dean
Faculty of Computing
August, 2025

Author's Declaration

I, **Saeed Abbas**, hereby state that my MPhil thesis titled "**The Extended Mode-Matching Method for a General Impedance Condition in Cylindrical Waveguide**" is my work and has not been submitted previously by me for taking any degree from Capital University of Science and Technology, Islamabad or anywhere else in the country/abroad.

At any time if my statement is found to be incorrect even after my graduation, the University has the right to withdraw my MPhil Degree.

(Saeed Abbas)

Registration No: MMT231014

Plagiarism Undertaking

I solemnly declare that the research work presented in this thesis is titled "**The Extended Mode-Matching Method for a General Impedance Condition in Cylindrical Waveguide**" is solely my research work with no significant contribution from any other person. Small contribution/help wherever taken has been dully acknowledged and that complete thesis has been written by me.

I understand the zero tolerance policy of the HEC and Capital University of Science and Technology towards plagiarism. Therefore, I as an author of the above-titled thesis declare that no portion of my thesis has been plagiarized and any material used as reference is properly referred/cited.

I undertake that if I am found guilty of any formal plagiarism in the above-titled thesis even after awarded of MPhil Degree, the University reserves the right to withdraw/revoke my MPhil degree and that HEC and the University have the right to publish my name on the HEC/University website on which names of students are placed who submitted plagiarized work.

(Saeed Abbas)

Registration No: MMT231014

Acknowledgement

I got no words to articulate my cordial sense of gratitude to **Almighty Allah** who is the most merciful and most beneficent to his creation.

I also express my gratitude to the last prophet of **Almighty Allah, Prophet Muhammad (PBUH)** the supreme reformer of the world and knowledge for a human being.

I would like to be thankful to all those who provided support and encouraged me during this work.

I would like to be grateful to my thesis supervisor **Dr. Muhammad Afzal**, for guiding and encouraging me in writing this thesis. It would have remained incomplete without his endeavours. Due to his efforts, I was able to write and complete this assertation.

I would like to pay great tribute to my **parents**, for their prayers, moral support, encouragement and appreciation.

Last but not the least, I want to express my gratitude to my **friends** who helped me throughout my MPhil degree.

(Saeed Abbas)

Abstract

This thesis investigates the propagation of acoustic waves in waveguides with varying impedance conditions, focusing on the effects of exceptional points (EP_2) and the coupling of symmetric and anti-symmetric modes. An extended mode-matching method is applied to analyze the complex wave behavior in systems bounded by rigid and soft closed ends. The problem is solved numerically by truncating the solution after considering a sufficient number of modes to capture the essential physics while maintaining computational efficiency. The analysis reveals that at lower frequencies, the scattering behavior is dominated by the fundamental mode, whereas higher frequencies excite additional modes, leading to intricate interference patterns. The agreement between the computed pressure and velocity profiles at the interface confirms the reliability of the extended mode-matching approach in handling complex impedance conditions. The findings provide valuable insights into wave propagation in structured waveguides, highlighting the importance of exceptional points and impedance conditions in shaping the modal behavior of the system.

Contents

List of Figures

Abbreviations

BVP	Boundary Value Problem
EP	Exceptional Point
HVAC	Heating, Ventilation and Air conditioning
MM	Mode-Matching
SMM	Standard Mode Matching

Symbols

c	Speed of sound
C_p	Constant pressure
C_v	Constant volume
k	Wave number
u	Flow velocity
∇	Gradient sign
τ	Stress tensor
α	Transverse wavenumber
g	Gravitational acceleration
p	Instantaneous pressure
p_0	Equilibrium pressure
T	Temperature
ω	Frequency
ϱ	Instantaneous density
ϱ_0	Equilibrium density
r	Specific gas constant
ϱg	Body forces
∇_p	Exerting force
γ	Ratio of specific heat
β	Bulk modulus
ϕ	Fluid velocity potential
ν	Upper wall parameter
μ	Lower wall parameter
Z	Impedance

a	Radius
η_n	Axial wavenumber
δ_{mn}	Kronecker delta

Chapter 1

Introduction and Literature Review

1.1 Introduction

Acoustics is the study of sound and vibrations in gases, solids, and liquids. Long ago, it helped design public spaces like stadiums and concert halls to control sound. Today, acoustics is used in many areas, including medicine, architecture, engineering, and music. It has become a vital part of various scientific fields and applications. Noise is a big problem today. It comes from things like air conditioning systems, power plants, cars, and other machines. This unwanted noise travels through pipes or channels. To reduce it, special materials that absorb sound and specially designed pipes or channels are used.

This research project uses mathematics to study how sound waves behave when they hit a special material inside a duct. It also explores how a wire mesh inside the duct affects the sound waves, creating interesting effects like changing the way the waves travel and the frequencies they can reach.

Helmholtz equations are used to solve a fundamental problem in physics with specific boundary conditions. Researchers have discovered that exceptional points, where multiple mode converge, are crucial for achieving maximum noise reduction

in acoustic waveguides. A new approach has been developed to handle these exceptional points, demonstrating numerical robustness and validity. This enhanced method has the potential for broad applications in fields involving complex symmetric operators.

Lawrie et al. [1] studied the analytic Mode-Matching technique for accurately handling exceptional points in lined acoustic waveguides. Exceptional points occur where the waveguide's mode coalesce, leading to singularities in the scattering matrix. The proposed method provides a robust and efficient way to compute the scattering matrix and handle these singularities.

Exceptional points are special degeneracies in non-Hermitian systems where two or more eigenvalues and their corresponding eigenvectors coalesce. Understanding these points is crucial in various applications, including optical systems, acoustics, and quantum mechanics.

Doe and Smith [2] introducing the theoretical background of wave scattering, explaining how waves interact with different structures and how their behavior can be described mathematically. Using Mode-Matching techniques, we formulated the problem in terms of eigenvalues and eigenfunctions, which allowed us to study the emergence of EPs systematically.

By utilizing the symmetric and antisymmetric operator concepts, researchers can better understand and analyze the behavior of exceptional points in acoustic waveguides, ultimately leading to improved noise reduction techniques.

The original work was conducted in rectangular coordinates, but I transitioned to cylindrical coordinates to analyze the problem. By applying rigid and soft boundary conditions, I solved the Helmholtz equation to study how sound waves reflect off a rigid wall and are absorbed in a soft medium. In this framework, the rigid boundary condition enforces a zero particle velocity, causing perfect reflection of sound waves, while the soft boundary condition allows for wave absorption due to the pressure release mechanism. This approach provides a clearer understanding of wave behavior in different media, particularly in cylindrical geometries where symmetry simplifies the analysis. The results demonstrate the distinct acoustic responses under rigid and soft conditions, highlighting reflection and absorption characteristics in wave propagation.

1.2 Literature Review

This study explores the behavior of acoustic waves as they propagate and scatter within cylindrical waveguides, analyzing their transmission and reflection properties. To mitigate unwanted noise, researchers propose optimizing acoustic waveguides by integrating sound-absorbing materials and strategically placing reactive liners.

B. J. Tester. [3] presented a seminal study on optimizing sound attenuation in ducts without mean flow. The author, B.J. Tester, investigates the attenuation of sound waves in ducts using a modal analysis approach. Novotny et al. [4] studied the problems in scanning near-field optical microscopy, we discuss light propagation in circular dielectric waveguides with finite aluminum cladding. In order to understand the origin of the different solutions, optical modes are first investigated for the dielectric waveguide with infinite aluminum cladding and for the aluminum cylinder. For aluminum a plasma dispersion law is assumed, leading to complex dielectric constants with negative real parts and to generally complex propagation constants. The dependence of the dispersion on the geometry and on the frequency is discussed for the various kinds of modes.

SW. Rienstra. [5] presented the number and location of the surface waves depends on the wall impedance Z and mean flow Mach number. When Z is varied, an acoustic mode may change via small transition zones into a surface waves and vice versa. Compared to the acoustic modes, the surface waves behave—for example as a function of the wall impedance—rather differently as they have their own dynamics. They are therefore more difficult to find. A method is described to trace all modes by continuation in Z from the hard-wall values, by starting in an area of the complex Z-plane without surface waves.. The other approach employs analytical techniques, which involve calculating dispersion relation roots and enforcing orthogonality to ensure acoustic field continuity at the silencer's boundaries, thereby predicting its acoustic behavior. Brambley and peake [6] presented a classification of surface modes in cylindrical lined ducts that are relevant to aeroacoustics. The authors, Edward J. Brambley and Nigel Peake, investigate

the properties of these modes, which are essential for understanding sound propagation and attenuation in ducts. Benmddour et al. [7] Results obtained for a vertical free-end cylinder are in good agreement with those published in the literature. Moreover, first results of the interaction of the fundamental compressional, flexural and torsional Pochhammer–Chree modes with non-axisymmetric vertical cracks are obtained and discussed. Then, the interactions of the fundamental compressional mode with oblique free-ends and cracks are briefly addressed. The power balance is shown to be satisfied with a good accuracy.

Graefe and Jones [8] investigate the behavior of optical lattices with a sinusoidal potential, which are symmetric. They focus on the threshold where the symmetry breaks, leading to a transition from a stable to an unstable regime. Bi and Pagneux [9] explored the behavior of modes in waveguides with impedance boundary conditions. The authors provide new insights into the properties of these modes, which are essential for understanding wave propagation in various fields, such as acoustics, electromagnetics, and quantum mechanics. Felix et al. [10] developed a numerical approach that accurately captures the complex behavior of acoustic waves in waveguides with impedance boundaries.

Afzal and Bilal [11] explored the understanding of acoustic wave behavior in complex geometries and has implications for the design of acoustic devices, such as filters, resonators, and sound absorbers. Goldzak et al. [12] developed the unique properties of exceptional points, where the usual rules of wave propagation are broken.

Kelsten [13] investigated a method for filtering higher-order acoustic modes using a resistive layer is proposed and applied to a two-dimensional rectangular waveguide with a quiescent fluid. An analogue of Cremer's criterion is discussed and used to obtain the optimal modal attenuation of the non- planar waves while the plane wave is preserved. Numerical validation of the concept is performed for a straight waveguide and an abrupt expansion in a waveguide. Afzal et al. [14] presented the duct configuration is placed symmetrically about x-axis. The main concern is to determine scattered fields behavior in different duct regions subject to different material properties of the walled duct. Krasnok et al. [15] provide

a comprehensive understanding of the underlying physics and potential applications of light scattering anomalies. Qiu et al. [16] analyzed the application of the Cremer concept to annular ducts for optimal sound attenuation. The Cremer concept, developed by Ludwig Cremer, is a theoretical framework for designing acoustic systems with maximum sound attenuation.

Zhang et al. [17] conducted the analysis of the Cremer impedance at low frequencies, exploring its. Mathematical formulation and physical interpretation. Behavior in different frequency ranges. Relationship with other acoustic properties, such as sound absorption and transmission. Kransnok and Miri [18, 19] refined additional understanding of acoustic wave propagation at or near an exceptional point EP is investigated in optics and photonics. Kirby and Duan [20] studied under certain conditions, a uniform mean flow is seen to significantly affect the phase speed for different eigenmodes, and it is shown that this may cause energy to transfer from the fluid to the surrounding wall at frequencies much lower than those seen without mean flow. This behaviour has the potential to increase sound radiation from ducts at lower frequencies when mean flow is present. Afzal et al. [21] established the scattering characteristics of non-planar trifurcated waveguides. The authors analyze the effects of non-planarity on the scattering properties of these waveguides. Ashida et at. [22] conducted an aims to provide a thorough understanding of non-Hermitian physics and its potential applications in various fields, such as quantum mechanics, condensed matter physics, and optics.

Guo et al. [23] conducted the behaviors of the least attenuated total sound power depend only on the lossy boundary conditions and frequency, but are independent of sources. The sound may be almost non-decaying along the waveguide transition region for any lossy impedance boundary conditions although all modes attenuate exponentially. This spatial transient appears particularly strongly if the impedance is close to an exceptional point of the propagator, at which a pair of adjacent modes achieve maximum attenuation predicted by Cremer optimum concept.

These results are confirmed using non-modal numerical calculations and a two-by-two toy model. Åbom and Jacob [24] commentary aims to clarify the proper

boundary conditions for the Cremer impedance, addressing potential misunderstandings or misapplications in previous research. Afzal et al. [25] presented an analysis of the traveling waveform in flexible waveguides containing absorbent material along flanged junctions. The authors investigate the effects of the absorbent material on the waveform propagation.

Bergholtz et al. [26] provided an in-depth exploration of the exceptional topology of non-Hermitian systems, a rapidly evolving field that has garnered significant attention in recent years. Langthjem and Nakano [27] investigated acoustic trapped modes and their symmetry properties in a circular cylindrical waveguide with a cavity. The researchers employ a mode-matching approach to analyze the waveguide and cavity system. Afzal and Shafique [28] investigated the traveling waveform of a flexible waveguide bounded by elastic plates and with an inserted expansion chamber having flanges at two junctions and a finite elastic membrane atop is investigated through a mode-matching method. Afzal et al. [29] investigated the understanding of wave propagation and scattering in complex waveguide structures, which is essential for the design and optimization of various devices, such as filters, antennas, and sensors.

Afsar and Alam [30] illustrated a mode-matching analysis of a flexural trifurcated waveguide, considering the effects of porosity. The researchers investigate the interaction between the waveguide and a fluid filling the material's pores, focusing on acoustic wave propagation. Kononchuk et al. [31] researched a novel accelerometer design based on exceptional points, which enhances the signal-to-noise ratio. The researchers demonstrate the device's performance using experiments and theoretical modeling. Duggan et al. [32] discussed the limitations of sensing at an exceptional point, a phenomenon that has gained attention for its potential applications in sensing and metrology. The researchers review the concept of exceptional points and investigate the fundamental limits of sensing at these points. Li et al. [33] demonstrated a deep learning-based inverse analysis method for higher order modes in a monocone TEM (Transverse Electromagnetic) cell.

Farooqui et al. [34] analyze varying the relative phase of two counterpropagating (normal or oblique) incident waves, the absorption due to wire mesh can be tuned from zero to unity. Experimental as well as numerical results demonstrate that this

phenomenon is extremely broadband—allowing, for instance, the symmetrization of the acoustic wave with a short pulse in the time domain. Tiryakioglu and Ozturk [35] executed a mode-matching analysis for sound propagation in a cylindrical duct with a partial lining. The researchers investigate the sound wave propagation along the cylindrical duct using mode-matching techniques.

Alruwaili et al. [36] investigated wave propagation and attenuation in cylindrical waveguides with flexible shells and acoustic liners. The study focuses on understanding wave scattering and attenuation in these types of waveguides. Nawaz et al. [37] presented a mode-matching analysis for understanding wave propagation in flexible shells and waveguides. Dai et al. [38] presented an efficient computational method, Spectral Numerical Mode Matching (SNMM), for analyzing electromagnetic waves in cylindrical geometries. Yang and Seong [39] investigated the acoustic transmission loss of a cylindrical silencer filled with multilayer poroelastic materials. The researchers use the mode-matching method to analyze the sound transmission problems in waveguides. Lu et al. [40] presented the realization of acoustic rainbow trapping within a three-dimensional context by incorporating corrugated grooves in a cylindrical waveguide.

1.3 Thesis Contribution

This research advances the study of acoustic wave propagation by transitioning the analysis from conventional rectangular coordinates to cylindrical coordinates, which more accurately represent practical waveguide geometries such as pipes and ducts. Within this cylindrical framework, the Helmholtz equation was solved under two distinct boundary conditions to investigate fundamental wave behaviors. The rigid boundary condition, enforcing zero particle velocity at the waveguide walls, models perfectly reflective surfaces and results in complete wave reflection with preserved acoustic energy - mathematically represented by the Neumann boundary condition. In contrast, the soft (pressure-release) boundary condition, characterized by zero acoustic pressure at the boundaries, simulates absorptive surfaces and leads to wave energy dissipation through the Dirichlet boundary condition.

The cylindrical coordinate system proved particularly advantageous as its inherent rotational symmetry simplified the mathematical treatment while maintaining physical accuracy, allowing solutions to be expressed in terms of Bessel functions for radial dependence and trigonometric functions for angular dependence. This analytical approach revealed significant differences in wave propagation characteristics: rigid boundaries produced distinct standing wave patterns with pressure antinodes at reflection points, while soft boundaries demonstrated damped propagating waves with energy absorption. The study further identified how cylindrical geometry introduces unique dispersion effects not present in rectangular systems, particularly in the coupling and splitting of waveguide modes. These findings provide crucial insights for optimizing noise control in practical applications such as ventilation systems and industrial piping, where understanding the interplay between geometric configuration and boundary conditions is essential for effective acoustic management. The research establishes a comprehensive theoretical foundation for analyzing waveguides with circular cross-sections and demonstrates the importance of coordinate system selection in acoustic modeling.

Our research on lined acoustic waveguides is structured as follows:

- **Chapter-1**, provides an introduction to the topic, discuss its historical context, and review relevant literature.

- In **Chapter-2**, fundamental definitions and key terms related to the subject are defined and explained.

- In **Chapter-3**, a comprehensive solution methodology for plane wave propagation is presented, incorporating general lining conditions on boundary walls. The approach encompasses both standard mode matching and enhanced mode matching techniques.

- In **Chapter-4**, an analytical solution is presented for plane wave propagation in a duct with embedded lining conditions, considering both rigid and soft duct configurations. The solution leverages standard mode matching

and enhanced mode matching techniques to accurately capture the wave propagation characteristics. Both the boundary value problems of chapter-3 and chapter-4 are solved by using the mode-matching technique.

- **Chapter-5** provides the summary and concluding remarks of the thesis. References used in the thesis are mentioned in **Bibliography**.

Chapter 2

Preliminaries

The objective of this chapter is to define some basic concepts that are useful to understand the work done in the following chapter.

2.1 Waves

A wave is a traveling disturbance that propagates through a medium, conveying energy as particles oscillate and change position. A key characteristic of waves is that they transmit energy, not physical matter itself. Classic examples of waves include sound waves, water waves, and light waves, which demonstrate this fundamental principle. Depends on the properties of the medium and the energy's transmission, waves can be divided into the following four classes.

(i) Mechanical Waves

Waves that require a physical medium to propagate, transfer energy through vibration or oscillation of particles are called mechanical waves. Examples include sound waves, water waves, and vibrations in solids, gases, and liquid.

(ii) Longitudinal Waves

The waves whose propagation in the direction of parallel to that of the medium's particle orientation are called longitudinal waves. Sound and pressure waves are two examples.

(iii) Transverse Waves

Transverse waves are characterized by particle motion that is perpendicular to the direction of wave propagation.

(iv) Electromagnetic Waves

Electromagnetic waves are generated when electric and magnetic fields oscillate at right angles to each other. Notably, these waves can propagate through a vacuum, eliminating the need for a physical medium to transfer energy. Examples of electromagnetic waves include radio waves, X-rays, and other forms of electromagnetic radiation.

2.2 Acoustics Overview

Acoustics encompasses the study of how mechanical waves travel through material. It explores how sound energy is produced, reflected, and transmitted within a medium. Its name originates from the Greek term acoustics, meaning related to hearing. The human auditory range typically spans from $20Hz$ to $20,000Hz, (20kHz)$, with sounds below $20Hz$ classified as infra-sound and those above $20kHz$ classified as ultrasound, both of which are beyond the range of human hearing.

2.2.1 Acoustic Wave Equation

The acoustic wave propagation in certain medium can be described mathematically in term of equations, known as acoustic wave equation. This equation can be obtained from the physical laws of motion and equation of state. The derivation is explained in the next subsections.

2.2.2 Conservation of Mass

The equation of mass conservation describes the balance between the net flux of mass and the rate of change of mass density, highlighting the fundamental principle

of mass conservation in a system. this topic is taken from book [41]

$$\frac{\partial \varrho}{\partial t} + \bigtriangledown.(\varrho v) = 0, \tag{2.1}$$

where v is the velocity of the flow and ϱ is the instantaneous density of mass.

2.2.3 Conservation of Momentum

The momentum conservation equation describes the net rate of momentum transfer to the forces acting on a system, describing how momentum is conserved in the presence of external forces.

$$\frac{\partial(\varrho v)}{\partial t} = - \bigtriangledown .(\varrho v)v - \bigtriangledown p + \varrho g. \tag{2.2}$$

Here p is the pressure, g is the acceleration due to gravity, $\bigtriangledown p$ denotes the exerting force and ϱg shows the body force.

From the above equation,

$$\frac{\partial(\varrho v)}{\partial t} + \bigtriangledown.(\varrho v)v = - \bigtriangledown p + \varrho g, \tag{2.3}$$

which implies that

$$\left(\frac{\partial \varrho}{\partial t} + \bigtriangledown.(\varrho v)\right) v = \varrho \left(\frac{\partial}{\partial t} + v.\bigtriangledown\right) v = - \bigtriangledown p + \varrho g. \tag{2.4}$$

Using the continuity condition, we can write

$$\varrho \frac{Dv}{Dt} = - \bigtriangledown p + \varrho g, \tag{2.5}$$

here $\frac{D}{Dt} = \frac{\partial}{\partial t} + v.\bigtriangledown$ is the total time derivative known as Stokes total time derivative contains first term to be time derivative and second term the convective term [42].

2.2.4 Equation of State

The thermodynamic behaviour of compressible fluid can be describe by the equation of state.
For the perfect gas, the equation of state is

$$p = \varrho r T, \tag{2.6}$$

here T used for temperature, and r gives specific gas constant. For a gas enclosed in a vessel of highly thermally conductive walls, the perfect gas isotherm can be given by

$$\frac{p}{p_0} = \frac{\varrho}{\varrho_0}, \tag{2.7}$$

here ϱ_0 and p_0 are the static density and pressure respectively. When no heat loss or gained by the system then perfect adiabatic is

$$\frac{p}{p_0} = \left(\frac{\varrho}{\varrho_0}\right)^{\gamma}, \tag{2.8}$$

here, γ is the ratio of specific heat at constant pressure C_p to the specific heat at constant volume C_v i.e,

$$\gamma = \frac{C_p}{C_v}.$$

The compression and rarefaction in a gas can be defined as condensation i.e

$$s = \frac{\varrho - \varrho_0}{\varrho_0}, \tag{2.9}$$

which yields

$$\varrho = \varrho_0(1 + s). \tag{2.10}$$

Using (2.10) into (2.8), we find

$$\frac{p}{p_0} = (1 + s)^{\gamma}. \tag{2.11}$$

Expanding the right hand side of above equation by using Taylor's series

$$\frac{p}{p_0} = 1 + \gamma s + \frac{\gamma(\gamma-1)}{2fic}s^2 + \cdots \tag{2.12}$$

For linear relationship

$$\frac{p}{p_0} \approx 1 + \gamma s + O(s^2), \tag{2.13}$$

or

$$\frac{p}{p_0} \approx 1 + \gamma s, \tag{2.14}$$

or

$$p - p_0 = \gamma p_0 s. \tag{2.15}$$

A distinct methodology for establishing the adiabatic connection between pressure and density fluctuations entails expressing pressure as a power series expansion about the equilibrium density, which can be alternatively formulated as:

$$p = p(h_0) + \left(\frac{\partial p}{\partial h}\right) h = h_0(h - h_0) + \left(\frac{\partial^2 p}{\partial h^2}\right) h = h_0(\varrho - \varrho_0)\cdots \tag{2.16}$$

or

$$p \approx p(h_0) + \left(\frac{\partial p}{\partial h}\right)_{h=h_0} (h - h_0), \tag{2.17}$$

or

$$p - p_0 = \left(\frac{\partial p}{\partial h}\right)_{h=h_0} (h - h_0). \tag{2.18}$$

Now, comparing (2.15) and (2.18), we find

$$\gamma = \frac{\beta}{h}, \tag{2.19}$$

where, $\beta = h_0 \left(\frac{\partial p}{\partial h}\right)_{h=h_0}$, the acoustic pressure at any point can be defined as,

$$P = p - p_0. \tag{2.20}$$

Additionally, (2.18) allows us to define the acoustic pressure as:

$$P = \beta s. \tag{2.21}$$

2.2.5 Velocity

In a cylindrical waveguide, velocity refers to how fast electromagnetic waves travel through the guide. There are two main types of velocity to consider phase velocity and group velocity. Phase velocity is the speed at which wave crests move in the guide, and it can be greater than the speed of light in free space. Group velocity is the speed at which the signal or energy travels down the waveguide, and it is typically less than the speed of light. These velocities in waveguides differ from waves traveling in free space and can vary based on the waveguide mode and signal frequency.

2.2.6 Pressure

Pressure is a scalar quantity that measures the force per unit area exerted perpendicular to a surface. It describes how a force is distributed over a given area and is a fundamental concept in physics, engineering, and fluid dynamics.

2.3 Derivation of Helmholtz Equation

The Helmholtz equation is a partial differential equation that can be derived from the wave equation. Here's a step-by-step derivation from the wave equation:

The wave equation describes the propagation of waves in a medium:

$$\frac{\partial^2 \phi}{\partial t^2} = c^2 \nabla^2 \phi \tag{2.22}$$

where $\phi(r, z, t)$ is the wave function, c is the speed of the wave, and ∇^2 is the Laplace operator. We assume that the wave function $\phi(x, y, z, t)$ can be written as:

$$\phi(r, z, t) = \varphi(r, z) e^{-i\omega t} \tag{2.23}$$

where $\varphi(r, z)$ is the spatial part of the wave function, ω is the angular frequency, and t is time.

Substituting the assumed solution into the wave equation, we get:

$$\frac{\partial^2}{\partial t^2}(\varphi(r,z)e^{-i\omega t}) = c^2\nabla^2(\varphi(r,z)e^{-i\omega t}). \tag{2.24}$$

Simplifying the left-hand side of equation (2.24) we get:

$$-\omega^2\varphi(r,z)e^{-i\omega t} = c^2\nabla^2\varphi(r,z)e^{-i\omega t}. \tag{2.25}$$

Canceling the exponential term $e^{-i\omega t}$ on both sides of equation (2.25), we get:

$$-\omega^2\varphi(r,z) = c^2\nabla^2\varphi(r,z) \tag{2.26}$$

Rearranging the equation (2.26), we get:

$$\nabla^2\varphi(r,z) + \frac{\omega^2}{c^2}\varphi(r,z) = 0. \tag{2.27}$$

Defining the wave number k as:

$$k = \frac{\omega}{c}, \tag{2.28}$$

we can rewrite the equation (2.27) as:

$$\nabla^2\varphi(r,z) + k^2\varphi(r,z) = 0. \tag{2.29}$$

The equation (2.29) is called the Helmholtz equation, which describes the spatial distribution of waves in a medium.

$$\nabla^2\varphi + k^2\varphi = 0. \tag{2.30}$$

The Helmholtz equation is a fundamental equation in many fields, including physics, engineering, and mathematics. It has numerous applications in wave propagation and scattering.

2.4 Boundary Conditions

The following boundary conditions are defined to model the BVPs,

1. Soft Conditions,

2. Rigid Conditions,

3. Impedance Conditions,

4. Fixed Conditions.

2.4.1 Soft Conditions

The soft boundary conditions are Dirichlet's type boundary conditions. In these conditions, the pressure is taken as zero, i.e.

$$\Phi(x_1, y_1) = 0,$$

2.4.2 Rigid Conditions

Neumann's type boundary conditions are actually rigid boundary conditions. In rigid conditions, normal velocity is taken as zero,

$$\frac{\partial \psi}{\partial x} = 0. \tag{2.31}$$

2.4.3 Impedance Conditions

The impedance boundary conditions are Robin's type boundary conditions. Robin boundary conditions are combination of Dirichlet boundary conditions and Neumann boundary conditions. These conditions are written as

$$\beta_1 \Phi(x_1, y_1) + \beta_2 \frac{\partial \psi(x_1, y_1)}{\partial x_1} = 0,$$

where β_1 and β_2 are arbitrary constants.

2.4.4 Fixed Conditions

In a waveguide, a fixed condition, also known as a fixed boundary or clamped boundary, is a boundary where,

- the displacement (movement) is zero,
- the wave-field is not allowed to move or vibrate,
- the boundary is rigid and immovable.

2.5 Superposition Principle

The superposition principle in wave fields states that when two or more waves overlap in space and time, the resulting wave is the sum of the individual waves. This means that the displacement of the medium at any point is the vector sum of the displacements caused by each wave. In other words, the waves add together, resulting in a new wave pattern.
This principle applies to all types of waves, including sound waves, light waves, and water waves. The superposition principle is a fundamental concept in wave physics and is used to explain a wide range of phenomena, including interference, diffraction, and wave propagation. It allows us to predict the behavior of complex wave systems by analyzing the individual waves and their interactions.

2.6 Mode-Matching Techniques

Numerous analytical strategies had been developed to investigate the reflection, transmission and absorption of waves in waveguides. The choice of such strategies subjected to material and geometrical properties of the guiding structures as well as the governing system of the physical problem.

Mode-Matching (MM) technique one of the most frequently employed methods for the problems containing structural discontinuities and different distribution of

impedance along the surfaces .

This technique is primarily based on the determination of field potentials in segments of guiding structure. Those expansions contain unknown amplitudes. The matching of pressures and velocities at interfaces converts the differential system into linear algebraic systems. Those systems are truncated and solved for the unknown amplitudes.

The applications of physical problems that are manageable by using MM technique are found in automobile industry, heating ventilation and air conditioning systems HVAC of buildings and engineering structures. The key elements in HVAC or automobile industry is a duct like structure. This structure transfer vibrational energy to the environment which is sometime described as noise.

Thus the designs of such elements that help to minimize noise are significant. Sometime these designs involve different geometric variations together with different material properties inside of the structures. The solution of such governing boundary value problems found against the physical problem of interest is not always easy to compute. However the MM technique which is relatively an easy approach gives an interesting method forward to find the solution of such problems. Some of such solutions are explained in the next chapters 3 and 4.

2.7 Standard Mode-Matching

The conventional Mode-Matching method is a mathematical framework employed to compute wave amplitude values in diverse physical systems, encompassing both electromagnetic and acoustic waveguides.

This method involves segmenting the system into separate regions and expressing the wave fields in each region as a series of modes. By enforcing boundary conditions at the interfaces between regions, a set of equations is obtained that links the amplitude coefficients of adjacent modes. Solving these equations yields the amplitude values, allowing for the calculation of wave fields throughout the system. This technique is invaluable for analyzing wave propagation in complex systems with discontinuous or rapidly changing wave fields, providing a robust mathematical framework for accurate modeling and simulation of wave-based phenomena.

2.8 Extended Mode-Matching

Extended Mode-Matching techniques offer a powerful mathematical tool for resolving unknown parameters in intricate physical systems. By combining cutting-edge numerical methods with traditional mode matching, these techniques deliver precise calculations of previously unknown variables.

The process involves subdividing the system into discrete regions, expressing wave fields as a series of modes, and deriving a system of equations based on boundary conditions.

To refine accuracy, sophisticated numerical methods such as optimization algorithms, iterative techniques, or perturbation methods are applied, enabling efficient solution of the equations and yielding unknown values with high precision. This enhanced technique is especially valuable for analyzing complex systems with multiple unknowns, nonlinear effects, or uncertain parameters, providing a robust mathematical framework for accurate modeling, simulation, and optimization of physical phenomena.

2.9 Exceptional Point of a Wave

Exceptional points, where multiple modes converge, have been recognized as optimal conditions for attenuation in lined acoustic waveguides. Recently, researchers have focused on designing liners that create exceptional points (EP_s) at specific frequencies to enhance sound absorption.

However, analytical modeling of acoustic scattering near exceptional points remains underdeveloped, with existing studies largely relying on standard methods that are only applicable near (EP) conditions.

When the root of the input equation equals zero, the coupled modes' dispersion and line-width converge without any gap at the crossing point. This unique point is referred to as an exceptional point (EP), where the eigenvalues and eigenvectors merge, denoted as S_1

$$K(s_1) = 0 \quad K'(s_1) = 0. \tag{2.32}$$

Symmetry of Wave

A wave's symmetry refers to its ability to remain unchanged when transformed in a specific way. In the case of translational symmetry, the wave looks the same after being shifted along the direction of traveling. A wave function $\varphi(x, y)$ is said to have a symmetry if:

$$\varphi(x, y) = \varphi(x + \lambda, y), \tag{2.33}$$

where λ is a wavelength.

Antisymmetric of Wave

A relation R on a set A is antisymmetric if, whenever $(r, z) \in R$ and $(z, r) \in R$, then $r = z$. Alternatively, R is antisymmetric if for all r, $z \in A$, if $r \neq z$, then either $(r, z) \notin R$ or $(z, r) \notin R$.
A relation R fails to be antisymmetric if there exist distinct elements r, $z \in A$ such that $(r, z) \in R$ and $(z, r) \in R$.

Note: If a relation is not symmetric that does not mean it is antisymmetric as,

$$\varphi(r, z) = -\varphi(r + \lambda, z). \tag{2.34}$$

The following definitions are taken from [43] and [44].

Waveguide

A waveguide is a structure designed to direct waves, including electromagnetic and sound waves, while minimizing energy loss. By constraining the wave expansion to one or two dimensions, the waveguides geometry plays a crucial role in its functionality.
In the context of acoustics, a waveguide behaves similarly to a transmission line, enabling the efficient propagation of sound waves.

Amplitude

The amplitude of vibration denotes the maximum displacement of a vibrating body from its equilibrium position.

Time Period

The period of oscillation displaying the time taken by the vibrating body to complete one rotation of motion. The period of oscillation is also known as the time period and is denoted by, $T = \frac{2\pi}{\omega}$, where ω is called the angular frequency.

Frequency

Frequency is defined as the number of complete oscillations or cycles a wave completes per unit time. Mathematically, it is the reciprocal of the time period which is the time taken for one complete cycle of the wave.

$$f = \frac{1}{T}. \tag{2.35}$$

Chapter 3

The Extended Mode-Matching Method for a General Impedance Condition in Infinite Cylindrical Waveguide

This chapter explores problems involving exceptional points, focusing on a governing equation subject to rigid and impedance boundary conditions. The mode-matching technique is employed to derive solutions for scenarios with zero and two exceptional points. The chapter's structure is as follows: Section 3.1 introduces the boundary value problem, providing a detailed description and mathematical formulation. In section 3.2 we describe the solution methodology used to obtain the solution. In section 3.3 we present the numerical results obtained for the boundary value problem discussed above.

3.1 Problem Formulation

Consider an infinite cylindrical waveguide with a radius of $\hat{r} = \hat{a}$, as illustrated in Figure 3.1. The waveguide located at $\hat{z} = 0$, has its inner surface filled with a compressible fluid characterized by density ρ and sound speed c. The region $\hat{z} \leq 0$

is bounded by a rigid surface, while the semi-infinite region $\hat{z} \geq 0$ is subject to an impedance-type condition at the boundary $\hat{r} = \hat{a}$.

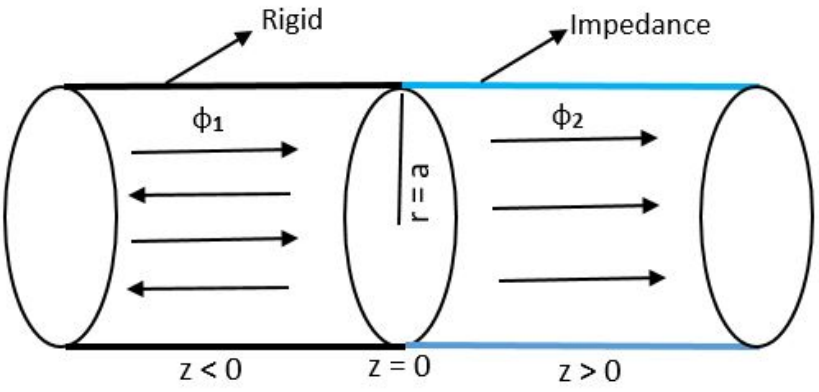

FIGURE 3.1: Diagram of the model problem

Note that a symbol hat is used to denote dimensional variables. The propagation of acoustic waves in fluids is governed by the wave equation

$$\frac{\partial^2 \hat{\Phi}}{\partial \hat{r}^2} + \frac{1}{\hat{r}} \frac{\partial \hat{\Phi}}{\partial \hat{r}} + \frac{\partial^2 \hat{\Phi}}{\partial \hat{z}^2} = \frac{1}{c^2} \frac{\partial^2 \hat{\Phi}}{\partial \hat{t}^2}. \tag{3.1}$$

Here $\hat{\Phi}$ is the fluid potential and the acoustic pressure $\hat{p}$ and velocity $\hat{v}$ are connected to the $\hat{\Phi}{=}\rho\frac{\partial \hat{\Phi}}{\partial \hat{t}}$ and $\hat{v} = \hat{\nabla}\hat{\Phi}$. The waveguide boundaries are rigid and of impedance type. The mathematical formulation of these boundary condition can be derived from the definition of acoustic impedance ($\hat{Z}$) which states that

$$\hat{Z} = \frac{\hat{P}}{\hat{\mathbf{n}}.\hat{\mathbf{v}}}. \tag{3.2}$$

Here $\hat{\mathbf{n}}$ is the unit vector directed normal to the surface, for rigid condition, $\hat{Z}$ is undefined, then (3.2) leads to:

$$\hat{\mathbf{n}}.\hat{\nabla}\hat{\Phi} = 0. \tag{3.3}$$

Thus at $\hat{z} \leq 0$ for $\hat{r} = \hat{a}$, the rigid condition can be expressed as:

$$\frac{\partial \hat{\Phi}}{\partial \hat{r}} = 0, \quad \hat{r} = a. \tag{3.4}$$

Where, for $\hat{z} \geq 0$, the impedance condition can be expressed as:

$$\hat{Z}\frac{\partial\hat{\Phi}}{\partial\hat{r}} = \rho\frac{\partial\hat{\Phi}}{\partial\hat{t}}, \quad \hat{r} = a. \tag{3.5}$$

Under the assumption of harmonic time dependence, the expression for $\hat{\Phi}$ can be express as:

$$\begin{cases} \hat{\Phi}(\hat{r},\hat{z},\hat{t}) = \varphi(\hat{r},\hat{z})e^{-i\omega\hat{t}}, \\ \hat{P}(\hat{r},\hat{z},\hat{t}) = \hat{p}(\hat{r},\hat{z})e^{-i\omega\hat{t}}, \\ \hat{V}(\hat{r},\hat{z},\hat{t}) = \hat{v}(\hat{r},\hat{z})e^{-i\omega\hat{t}}. \end{cases} \tag{3.6}$$

Applying transformation defined in the equations(3.6), (3.1) and (3.3)-(3.5) can be rewritten as:

- Helmholtz equation

$$\left\{\frac{\partial^2}{\partial\hat{r}^2} + \frac{1}{\hat{r}}\frac{\partial}{\partial\hat{r}} + \frac{\partial^2}{\partial\hat{z}^2} + \hat{k}^2\right\}\hat{\varphi}(\hat{r},\hat{z}) = 0. \tag{3.7}$$

- Rigid condition

$$\frac{\partial\hat{\varphi}}{\partial\hat{r}} = 0, \quad \hat{r} = \hat{a}. \tag{3.8}$$

- Impedance condition

$$\hat{Z}\frac{\partial\hat{\varphi}}{\partial\hat{r}} = -i\omega\rho\hat{\varphi}, \quad \hat{r} = \hat{a}. \tag{3.9}$$

The problem can be transformed by using dimensionless variables, that is,

$$\begin{cases} \hat{r} = ar, \\ \hat{z} = az, \\ \omega\hat{t} = t, \\ a^2\hat{\Phi} = \varphi. \end{cases} \tag{3.10}$$

Using the transformation given in equation (3.10), we obtain the dimensionless form

$$\left\{\frac{\partial^2}{\partial r^2}+\frac{1}{r}\frac{\partial}{\partial r}+\frac{\partial^2}{\partial z^2}+k^2\right\}\varphi(r,z)=0, \tag{3.11}$$

where, k denotes the wavenumber, defined as the ratio of angular frequency ω to the speed of sound c, i.e., $\frac{\omega}{c}$. In the context of the cylindrical waveguide, (φ_1) and (φ_2) generally represent the field potentials in two distinct regions. For this model, the rigid boundary condition is specified as:

$$\frac{\partial\varphi_1}{\partial r}=0, \quad r=a. \tag{3.12}$$

The duct region $z \geq 0$ is lined with acoustic material, and the following boundary condition apply in this region

$$\frac{\partial\varphi_2}{\partial r}+\mu\varphi_2=0, \quad r=a, \tag{3.13}$$

where

$$\mu=\frac{ic\rho ka}{Z_\mu}. \tag{3.14}$$

3.2 Mode-Matching Solutions

The rigid and soft boundary of the problem defined in equations (3.12) and (3.13) can be solved by using the mode matching technique. Due to the involvement of lined boundary conditions there exist exceptional points and there will exist standard and enhanced mode matching formulation in solution procedure. Thus the two formal action of solution are possible for the modelled setting.

- Standard mode-matching solution
- Extended mode-matching with two exceptional points

These solutions are further discuss in the following subsection.

3.2.1 Standard Mode-Matching Solution

The standard mode-matching form does not involve any exceptional points. For standard mode-matching we determine eigenfunction expansions by using the separation of variables method. We apply the separation of variables method by assuming a solution of the form:

$$\varphi_1(r,z) = R(r)Z(z). \tag{3.15}$$

Substituting (3.15) into (3.11), we can find

$$\frac{R''}{R} + \frac{1}{r}\frac{R'}{R} + \tau^2 = 0, \tag{3.16}$$

where τ is given as:

$$\tau = \sqrt{k^2 - s^2}. \tag{3.17}$$

Multiplying (3.16) with (r^2R), we obtain

$$r^2R'' + rR' + r^2\tau^2R = 0. \tag{3.18}$$

The solution of the Bessel differential equation (3.18), is

$$R(r) = C_3J_0(\tau r) + C_4N_0(\tau r), \tag{3.19}$$

where J_0 and N_0 are the Bessel function of first and second kind respectively.

Note that when $r \to 0$ the Bessel function of second kind becomes undefined, therefore at bounded domain the solution will be

$$R(r) = C_3J_0(\tau r). \tag{3.20}$$

Now, by applying the rigid boundary condition defined in (3.13) to (3.20), we obtain

$$J_0'(\tau r) = 0. \tag{3.21}$$

There are infinite many values of τ: $\tau_0, \tau_1, \cdots, \tau_n$ for which (3.21) holds. These values τ_n where $n = 0, 1, 2, 3, \cdots$ are known as eigenvalues and the corresponding eigenfunctions is

$$R_{1n}(r) = C_3 J_0(\tau_n r). \tag{3.22}$$

From (3.15), the solution of ordinary differential equation $Z(z)$ is

$$Z(z) = C_1 e^{i\eta_n z} + C_2 e^{-i\eta_n z}, \tag{3.23}$$

where

$$\eta_n = \sqrt{k^2 - \tau_n^2}. \tag{3.24}$$

The eigenfunctions R_{1n} and R_{1m} are orthogonal and satisfy the following orthogonality relation.

$$\delta_{nm} F_m = \int_0^a r R_m(r) R_n(r) \mathrm{dr}, \tag{3.25}$$

where (δ_{nm}) denotes the Kronecker delta. Here, C_1, C_2 and C_3 are arbitrary constants. Since there are infinitely many solutions, the superposition principle can be applied to formulate the eigenfunction expansion using (3.22) and (3.23).

Consequently, the equation (3.15) becomes

$$\varphi_1(r, z) = \sum_{n=0}^{\infty} F_n J_0(\tau_n, r) e^{i\eta_n z} + \sum_{n=0}^{\infty} A_n J_0(\tau_n, r) e^{-i\eta_n z}. \tag{3.26}$$

Thus, when the fundamental duct mode is treated as the incident mode, a simplified formulation emerges. To streamline the notation, wall parameters and wavenumbers will be presented without distinction, as the context will clearly convey the nature of the exceptional point (EP). The velocity potentials can be represented as eigenfunction expansions. Specifically, for the inlet duct, the expansion takes the following form

$$\varphi_1(r, z) = e^{ikz} + \sum_{n=0}^{\infty} A_n R_{1n}(r) e^{-i\eta_n z}. \tag{3.27}$$

A similar equation for $\varphi_2(r,z)$ can be written as:

$$\varphi_2(r,z) = \sum_{n=0}^{\infty} B_n R_{2n}(r) e^{is_n z} + \sum_{n=0}^{\infty} A_n R_{2n}(r) e^{-is_n z}. \tag{3.28}$$

As there is no reflection in the region at $x \geq 0$, thus $A_n = 0$, and equation (3.28) reduces to

$$\varphi_2(r,z) = \sum_{n=0}^{\infty} B_n R_{2n}(r) e^{is_n z}. \tag{3.29}$$

where A_n representing the reflected mode amplitudes and B_n representing the transmitted mode amplitude are still unknown for $n = 0, 1, 2, \cdots$. These are found by using mode-matching procedure.

The continuity of pressure at $z = 0$ by using standard mode-matching condition. The physical problems are governed by Helmholtz's equation along with the acoustic absorbing lining. The mode-matching method has been used to find the solution of these modelled problems. The duct's circular boundary surface is coated with an absorbing material.

$$\varphi_1(r,0) = \varphi_2(r,0). \tag{3.30}$$

Putting (3.27) and (3.29) into (3.30), we get

$$e^{ikz} + \sum_{n=0}^{\infty} A_n R_{1n}(r) e^{-i\eta_n z} = \sum_{n=0}^{\infty} B_n R_{2n}(r) e^{is_n z}. \tag{3.31}$$

Substituting $z = 0$ into (3.31), gives

$$e^{ik0} + \sum_{n=0}^{\infty} A_n R_{1n}(r) e^{-i\eta_0 0} = \sum_{n=0}^{\infty} B_n R_{2n}(r) e^{iS_n 0}, \tag{3.32}$$

or

$$1 + \sum_{n=0}^{\infty} A_n R_{1n}(r) = \sum_{n=0}^{\infty} B_n R_{2n}(r). \tag{3.33}$$

Multiplying (3.33) with $rR_{1m}(r)$ and then integrating from $0 < r < a$, we obtain

$$\begin{aligned}\int_0^a R_{1m}(r)r\mathrm{d}r + \sum_{n=0}^{\infty} A_n \int_0^a R_{1n}(r)rR_{1m}(r)\mathrm{d}r \\ = \sum_{n=0}^{\infty} B_n \int_0^a R_{1m}(r)R_{2n}(r)r\mathrm{d}r,\end{aligned} \tag{3.34}$$

or

$$\delta_{m0} + A_m = \frac{1}{E_m}\sum_{n=0}^{\infty} B_n P_{mn}. \tag{3.35}$$

The orthogonality relation is expressed as follows, yielding the expressions for P_{mn} and the Kronecker delta δ_{mn}:

$$\delta_{mn}E_m = \int_0^a R_{1n}(r)R_{1m}(r)r\mathrm{d}r, \tag{3.36}$$

$$P_{mn} = \int_0^a R_{1m}(r)R_{2n}(r)r\mathrm{d}r, \tag{3.37}$$

$$\delta_{m0} = \int_0^a R_{1m}(r)r\mathrm{d}r. \tag{3.38}$$

Following the simplification of (3.34), we obtain A_m

$$A_m = -\delta_{m0} + \frac{1}{E_m}\sum_{n=0}^{\infty} B_n P_{mn}. \tag{3.39}$$

Normal velocity refers to the fluid velocity component perpendicular to a surface or boundary. In acoustic wave propagation, normal velocity at the boundary is crucial for determining acoustic impedance and reflection coefficients. To ensure velocity field continuity, the mode matching technique involves matching normal velocities at the interface between adjacent regions or domains, a vital step in solving wave propagation problems. The normal velocity component is continuous at the boundary of the cylindrical waveguide, which implies that

$$\varphi_{2z}(r,0) = \varphi_{1z}(r,0). \tag{3.40}$$

Putting (3.27) and (3.29) into (3.40), we get:

$$e^{ikz} + \sum_{n=0}^{\infty} A_n R_{1n}(r) e^{-i\eta_n z} = \sum_{n=0}^{\infty} B_n R_{2n}(r) e^{is_n z}. \tag{3.41}$$

Now, taking the derivatives of (φ_1) and (φ_2) with respect to z and substituting the results into (3.41), we obtain:

$$\sum_{n=0}^{\infty} B_n R_{2n}(r) i s_n e^{is_n z} = ike^{ikz} - \sum_{n=0}^{\infty} A_n R_{1n}(r) i\eta_n e^{i\eta_n z}. \tag{3.42}$$

Setting $z = 0$ in (3.42), the equation reduces to

$$\sum_{n=0}^{\infty} B_n i s_n R_{2n}(r) e^{iS_n 0} = ike^{ik0} - \sum_{n=0}^{\infty} A_n i\eta_n R_{1n}(r) e^{-i\eta_n 0}, \tag{3.43}$$

upon simplification, (3.43) becomes:

$$i\sum_{n=0}^{\infty} B_n s_n R_{2n}(r) = ik - i\sum_{n=0}^{\infty} A_n \eta_n R_{1n}(r). \tag{3.44}$$

Multiplying (3.44) with $rR_{2m}(r)$ and then integrating from $0 < r < a$, we obtain

$$\begin{aligned} i\sum_{n=0}^{\infty} B_n \int_0^a R_{2n}(r) R_{2m}(r) r\mathrm{d}r S_n = ik \int_0^a R_{2m}(r) r\mathrm{d}r \\ - i\sum_{n=0}^{\infty} A_n \eta_n \int_0^a R_{1n}(r) r R_{2m}(r)\mathrm{d}r, \end{aligned} \tag{3.45}$$

or

$$B_m \delta_{nm} F_m = k\delta_{0m} - \sum_{n=0}^{\infty} A_n \eta_n M_{nm}. \tag{3.46}$$

Orthogonality relation can be express as:

$$\delta_{nm} F_m = \int_0^a r R_{1n}(r) R_{1m}(r)\mathrm{d}r. \tag{3.47}$$

The values of E_m, δ_{nm}, and M_{nm} are express as:

$$E_m = \int_0^a R_{2m}^2(r) r\mathrm{d}r, \tag{3.48}$$

and

$$M_{nm} = \int_0^a R_{1n}(r) r R_{2m}(r) \mathrm{dr}. \tag{3.49}$$

This leads to

$$B_m = k\delta_{0m} - \frac{1}{F_m} \sum_{n=0}^{\infty} A_n \eta_n M_{nm}. \tag{3.50}$$

3.2.2 Extended Mode-Matching Solution with two Exceptional Points

At the exceptional point (EP) conditions, η_1 is a double root of $K(s) = 0$, and since $K'(s_1) = 0$, which implies $P_1 = 0$, $\chi(\tau_1, r)$ exhibits self-orthogonality, resulting in a degenerate system of equations. To accurately capture the transmitted wave field, an additional function is necessary. However, to maintain a straightforward structure for the EP eigenfunction expansion, it is advantageous to reformulate this waveform in terms of functions of z and their corresponding z-derivatives. An exceptional point (EP) occurs when there exists a specific value of S_n such that both the functions. τ_1 be the exceptional points there. The exceptional mode propagation can be given as

$$\varphi_2(\tau_1, r) = \frac{\partial}{\partial s}[R_{2n}(\tau_1, r) e^{is_1 z}], \tag{3.51}$$

which leads to

$$\varphi_2(\tau_1, r) = [\frac{\partial R_{2n}(\tau_1, r)}{\partial s} + izR_{2n}(\tau_1, r)] e^{is_1 z}, \tag{3.52}$$

where

$$\chi(\tau_1, r) = \frac{\partial R_{2n}(\tau_1, r)}{\partial s}. \tag{3.53}$$

Substituting (3.53) into (3.52) yields (3.54)

$$\begin{aligned} \varphi_2(r, z) = \bar{B}_1[-\frac{s_1}{\tau_1^2}\chi(\tau_1, r) + izR_{2n}(\tau_1, r)] e^{is_1 z} \\ + \sum_{n=0}^{\infty} B_n R_{2n}(\tau_n, r) e^{is_n z}. \end{aligned} \tag{3.54}$$

The overbar indicates that these are the values of the parameters at the exceptional point EP_2. At EP_2, the equation $K(s) = 0$ is satisfied, and since the derivative

$K'(s_1)$ also vanishes, the coefficient P_1 becomes zero, causing the eigenfunction $\chi(\tau, r)$ to become self-orthogonal.

3.2.2.1 Continuity of Pressure

In mode matching solutions, the continuity of pressure is enforced by matching the pressure fields at the interface between two regions. This is typically done by expanding the pressure fields in each region in terms of a set of basis functions (e.g., modes) and then matching the coefficients of these expansions at the interface. By enforcing the continuity of pressure, mode matching solutions can accurately capture the behavior of acoustic waves at interfaces and ensure that the resulting solutions are physically meaningful. The conditions of continuity of pressure is

$$\varphi_1(r, 0) = \varphi_2(r, 0). \tag{3.55}$$

Putting (3.27) and (3.54) into (3.55), we get:

$$\begin{aligned} e^{ikz} + \sum_{n=0}^{\infty} A_n R_{1n}(r, \tau_1) = \bar{B}_1[-\frac{s_1}{\tau_1^2}\chi(\tau_1, r) + izR_{2n}(\tau_1, r)]e^{is_1 z} \\ + \sum_{n=0}^{\infty} B_n R_{2n}(\tau_n, r)e^{is_n z}. \end{aligned} \tag{3.56}$$

Setting $z = 0$ into (3.56), we get:

$$\begin{aligned} e^{ik0} + \sum_{n=0}^{\infty} A_n R_{1n}(r, \tau_1) = \bar{B}_1[-\frac{s_1}{\tau_1^2}]\chi(r, \tau_1) + i(0)R_{2n}(r, \tau_1) \\ + \sum_{n=0}^{\infty} B_n R_{2n}(r, \tau_1)e^{is_n 0}. \end{aligned} \tag{3.57}$$

The (3.57) can be reduce to

$$1 + \sum_{n=0}^{\infty} A_n R_{1n}(r, \tau_1) = \bar{B}_1[-\frac{s_1}{\tau_1^2}]\chi(r, \tau_1) + \sum_{n=0}^{\infty} B_n R_{2n}(r, \tau_1). \tag{3.58}$$

Now, we multiply (3.58) with $R_{1m}(\tau, r)$ and integrating from $0 < r < a$, to obtain

$$\begin{aligned}&\int_0^a R_{1m}(r)r\mathrm{d}r + \sum_{n=0}^{\infty} A_n \int_0^a R_{1n}(r)R_{1m}(r)r\mathrm{d}r \\ &= \bar{B}_1[-\frac{s_1}{\tau_1^2}] \int_0^a R_{1m}(r)\chi(r,\tau)r\mathrm{d}r \\ &+ \sum_{n=0}^{\infty} B_n \int_0^a R_{2n}(r)R_{1m}(r)r\mathrm{d}r.\end{aligned} \tag{3.59}$$

Substituting $\delta_{m0}E_m$, P_{mn} and M_{0m} into (3.59), it reduces to

$$\delta_{m0}E_m + \sum_{n=0}^{\infty} A_n\delta_{mn}E_m = \bar{B}_1[-\frac{s_1}{\tau_1^2}]M_{0m} + \sum_{n=0}^{\infty} B_nP_{mn}. \tag{3.60}$$

Orthogonality relation can be express as:

$$\delta_{nm}F_m = \int_0^a rR_{1n}(r)R_{1m}(r)\mathrm{d}r. \tag{3.61}$$

We now express the values of $\delta_{nm}E_m$, M_{0m}, and P_{nm} as follows:

$$\delta_{om}E_m = \int_0^a R_{1m}(r)r\mathrm{d}r, \tag{3.62}$$

$$E_m = \int_0^a R_{1n}(r)R_{1m}(r)r\mathrm{d}r, \tag{3.63}$$

$$M_{m0} = \int_0^a rR_{1m}(r)\chi(r,\tau)\mathrm{d}r, \tag{3.64}$$

and

$$P_{mn} = \int_0^a rR_{2n}(r)R_{1m}(r)\mathrm{d}r, \tag{3.65}$$

$$\delta_{0m}E_m + A_mE_m = -\bar{B}_1\frac{s_1}{\tau_1^2}M_{0m} + \sum_{n=0}^{\infty} B_nP_{mn}, \tag{3.66}$$

$$A_mE_m = -\delta_{0m}E_m - \bar{B}_1\frac{s_1}{\tau_1^2}M_{0m} + \sum_{n=0}^{\infty} B_nP_{mn}. \tag{3.67}$$

The simplified form of (3.67), is

$$A_m = -\delta_{0m} - \bar{B}_1\frac{1}{E_m}\frac{s_1}{\tau_1^2}M_{0m} + \frac{1}{E_m}\sum_{n=0}^{\infty} B_nP_{mn}. \tag{3.68}$$

3.2.2.2 Continuity of Normal Velocity

We then apply the velocity continuity condition at $z = 0$, namely

$$\varphi_{2z}(r, 0) = \varphi_{1z}(r, 0). \tag{3.69}$$

Putting (3.27) and (3.54) into (3.69), we get:

$$\begin{aligned} e^{ikz} + \sum_{n=0}^{\infty} A_n R_{1n}(\tau_1, r) = \bar{B}_1[-\frac{s_1}{\tau_1^2}\chi(\tau_1, r) + izR_{2n}(\tau_1, r)]e^{is_1 z} \\ + \sum_{n=0}^{\infty} B_n R_{2n}(\tau_n, r)e^{is_n z}. \end{aligned} \tag{3.70}$$

Now taking the derivative of (3.70) with respect to z, we get

$$\begin{aligned} \bar{B}_1\left[-\frac{s_1}{\tau_1^2}\right] is_1 e^{is_1 z}\chi(\tau, r) + i^2 z s_1 R_{2n}(r)e^{is_1 z} + \sum_{n=0}^{\infty} B_n R_{2n}(r)e^{is_n z} is_n \\ = ike^{ikz} + \sum_{n=0}^{\infty} A_n R_{1n}(r)i\eta_n e^{i\eta_n z}. \end{aligned} \tag{3.71}$$

Substituting $z = 0$ into (3.71), and the resulting equation is

$$\begin{aligned} &\bar{B}_1\left[-\frac{s_1}{\tau_1^2}\right]\chi(\tau, r)iS_1 e^{is_1 0} + iR_{2n}(r)e^{is_1 0} + i^2 s_1(0)R_{2n}(r)e^{is_1 0} \\ &+ \sum_{n=0}^{\infty} B_n R_{2n}(r)is_n e^{is_n 0} = ike^{ik0} + \sum_{n=0}^{\infty} A_n R_{1n}(r)i\eta_n e^{i\eta_n 0}. \end{aligned} \tag{3.72}$$

Simplification leads to

$$\begin{aligned} \bar{B}_1\left[-\frac{s_1^2}{\tau_1^2}\right]\chi(\tau, r) + R_{2n}(r) + \sum_{n=0}^{\infty} s_n B_n R_{2n}(r) \\ = k - \sum_{n=0}^{\infty} A_n \eta_n R_{1n}(r). \end{aligned} \tag{3.73}$$

Multiplying (3.73) with $rR_{2m}(r)$ and then integrating over the interval $0 < r < a$, we obtain:

$$\begin{aligned}
&\bar{B}_1[-\frac{s_1^2}{\tau_1^2}]\int_0^a R_{2m}(r)\chi(r,\tau)r\mathrm{d}r + \int_0^a R_{2m}(r)R_{2n}(r)r\mathrm{d}r \\
&+\sum_{n=0}^{\infty} s_n B_n \int_0^a rR_{2m}(r)R_{2n}\mathrm{d}r\& = k\int_0^a R_{2m}(r)r\mathrm{d}r \\
&-\sum_{n=0}^{\infty} A_n\eta_n \int_0^a rR_{2m}(r)R_{1n}(r)\mathrm{d}r.
\end{aligned} \tag{3.74}$$

Further simplification of equation (3.74) express as:

$$\bar{B}_1[-\frac{s_1^2}{\tau_1^2}]M_{0m} + M_{mn} + \sum_{n=0}^{\infty} s_n B_n \delta_{mn} E_m = k\ell_{0m} - \sum_{n=0}^{\infty} A_n\eta_n H_{mn}. \tag{3.75}$$

We express the values of $\delta_{nm}E_m$, M_{0m}, M_{nm}, and H_{nm} as follows:

$$\delta_{mn}E_m = \int_0^a rR_{2m}(r)R_{2n}(r)\mathrm{d}r, \tag{3.76}$$

$$M_{0m} = \int_0^a R_{2m}(r)\chi(r,\tau)r\mathrm{d}r, \tag{3.77}$$

$$\ell_{0m} = \int_0^a rR_{2m}(r)\mathrm{d}r, \tag{3.78}$$

and

$$H_{mn} = \int_0^a rR_{2m}(r)R_{1n}(r)\mathrm{d}r. \tag{3.79}$$

The amplitude equation obtained is as follows:

$$B_m = k\delta_{0m}\frac{1}{s_n} - \frac{1}{s_n} + \bar{B}_1\left[\frac{s_1^2}{\tau_1^2}\right]\frac{1}{s_n E_m} - \frac{1}{s_n E_m}\sum_{n=0}^{\infty} A_n\eta_n H_{mn}. \tag{3.80}$$

The resulting system of linear algebraic equations is then truncated and solved simultaneously.

Multiplying (3.73) with $\chi(\tau, r)$ and then integrating from $0 < r < a$, reduce to equation (3.81) as:

$$\begin{aligned}\bar{B}_1[-\frac{s_1^2}{\tau_1^2}]\int_0^a \chi^2(r,\tau)r\mathrm{d}r + \int_0^a rR_{2n}(r)\chi(r,\tau)\mathrm{d}r \\ + \sum_{n=0}^{\infty} s_n B_n \int_0^a \chi(r,\tau)R_{2n}(r)r\mathrm{d}r \\ = k\int_0^a \chi(r,\tau)r\mathrm{d}r - \sum_{n=0}^{\infty} A_n\eta_n \int_0^a R_{1n}(r)r\chi(r,\tau)\mathrm{d}r.\end{aligned} \tag{3.81}$$

Orthogonality relation can be express as:

$$\delta_{nm}F_m = \int_0^a rR_{1n}(r)R_{1m}(r)(r)\mathrm{d}r \tag{3.82}$$

$$\bar{B}_1[-\frac{s_1^2}{\tau_1^2}H + M] + \sum_{n=0}^{\infty} s_n B_n Q = kM_0 - \sum_{n=0}^{\infty} A_n\eta_n L_{nm}. \tag{3.83}$$

We define the expression for H, M, Q, M_{0m} and ℓ_{0n} as follows:

$$H = \int_0^a \chi^2(r,\tau)r\mathrm{d}r, \tag{3.84}$$

$$M = \int_0^a R_{2n}(r)\chi(r,\tau)\mathrm{d}r, \tag{3.85}$$

$$Q = \int_0^a R_{2n}(r)r\chi(r,\tau)\mathrm{d}r, \tag{3.86}$$

$$M_0 = \int_0^a \chi(r,\tau)r\mathrm{d}r, \tag{3.87}$$

and

$$\ell_{nm} = \int_0^a R_{1n}(r)r\chi(r,\tau)\mathrm{d}r. \tag{3.88}$$

In a matrix notation by comparing the coefficients we can write the above equation (3.88) as follows:

$$\begin{bmatrix} S_1 Q & M - \dfrac{S_1^2}{\tau_1^2} H \\ 0 & -\dfrac{S_1^2}{\tau_1^2} \end{bmatrix} \begin{bmatrix} B_1 \\ \bar{B}_1 \end{bmatrix} = \begin{bmatrix} K M_0 - \sum_{n=0}^{\infty} A_n \eta_n \ell_{nm} \\ K \ell_{01} - \sum_{n=0}^{\infty} A_n \eta_n \ell_{n1} \end{bmatrix}. \tag{3.89}$$

3.3 Numerical Results

In this section, a detailed numerical discussion of the solution obtained in the previous section is presented. The systems are truncated by considering $n = 15$ terms, which ensures that the solution captures the essential modes while maintaining computational efficiency. The following parameter values are used in the analysis: the duct radius is taken as $a = 1\,\text{cm}$, the interface height is $h = 1\,\text{cm}$, the viscosity coefficient is $\mu = 1$, the speed of sound in air is $c = 343.5\,\text{m/s}$, and the air density is $\rho = 1.2$.

Figure 3.2 presents the real parts of the pressure as a function of the radius at $r = 0$ on the interface located at $z = 0$, considering different values of the frequency. It can be clearly observed that the real parts of the pressures in the regions $z < 0$ and $z > 0$ match exactly at the interface, which is consistent with the continuity condition of pressure. This agreement validates the accuracy of the truncated solution and confirms that the applied numerical approach is robust and reliable under varying frequency conditions.

Moreover, the results demonstrate that as the frequency increases, more modes are excited, leading to complex scattering behavior. At lower frequencies, the system exhibits a simpler scattering pattern dominated by the fundamental mode. However, as the frequency increases, higher-order modes are progressively excited, which introduces more intricate interference patterns and modifies the overall scattering characteristics. This behavior reflects the increased interaction of the incident waves with the boundary conditions and the structural geometry of the duct.

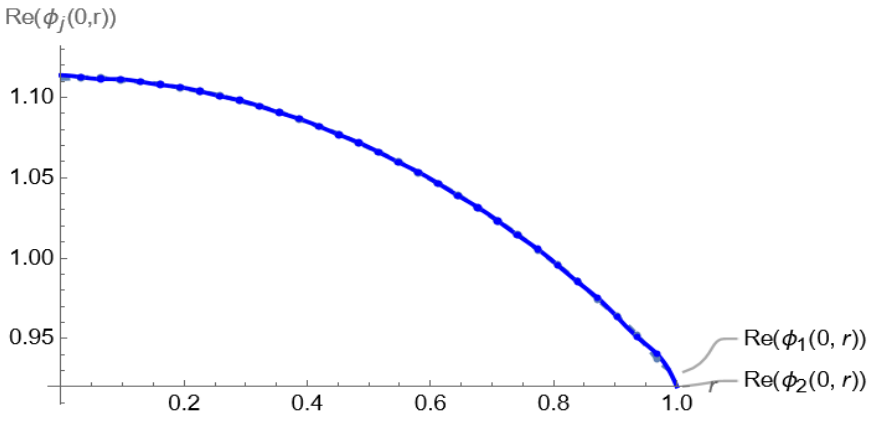

(a) $f = 50$ Hz

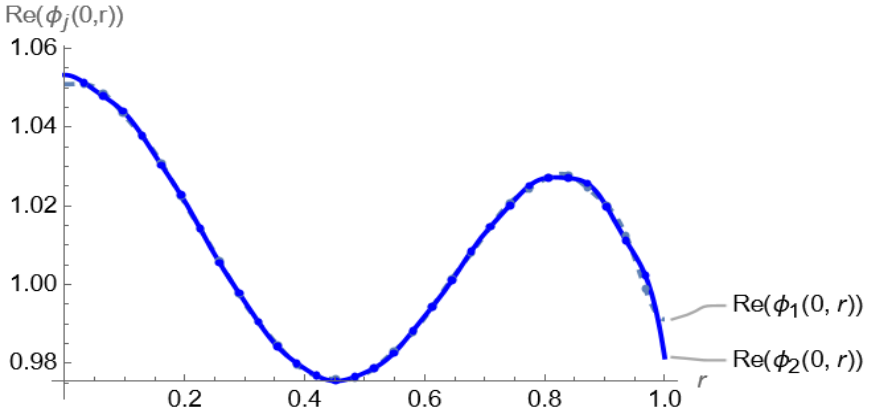

(b) $f = 500$ Hz

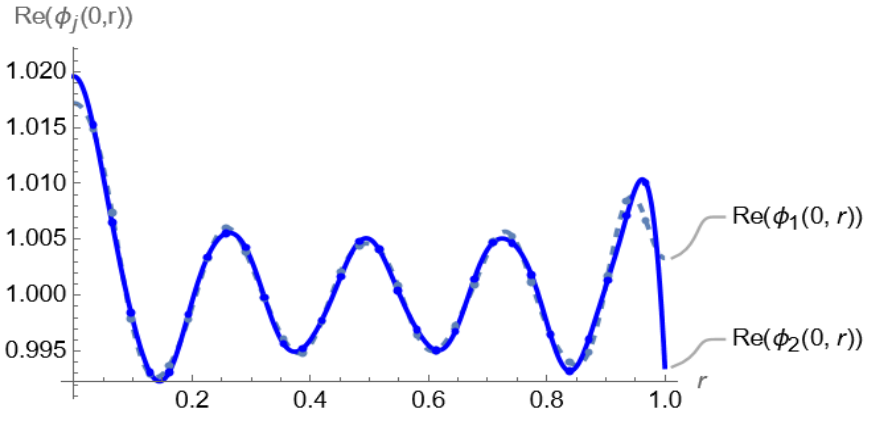

(c) $f = 1500$ Hz

FIGURE 3.2: Real parts of pressures versus radius r at interface $z = 0$, where $\mu = 1$ and $a = 1$.

Figure 3.3 shows the imaginary parts of the pressure versus the radius at $r = 0$ on the interface at $z = 0$ for different values of the frequency. Similarly to the real parts, the imaginary parts of the pressures in the regions $z < 0$ and $z > 0$ also

match exactly at the interface, which satisfies the continuity of pressure conditions. This agreement further confirms the accuracy of the truncated solution and the validity of the applied numerical approach.

The behavior of the imaginary parts of the pressure provides additional insight into the scattering mechanism. The imaginary part reflects the phase information of the scattered wave, which is crucial for understanding the overall wave behavior. As the frequency increases, the imaginary parts exhibit more complex patterns due to the increased contribution of higher-order modes. This complexity arises from the enhanced interaction between the incident wave and the duct geometry, leading to more pronounced scattering effects. Figure 3.4 presents the real parts of the velocity as a function of the radius at $r = 0$ on the interface at $z = 0$ for different frequency values. It can be observed that the real parts of the velocities in the regions $z < 0$ and $z > 0$ match exactly at the interface, which is consistent with the continuity condition of velocity. This agreement validates the accuracy of the truncated solution and demonstrates that the numerical approach effectively satisfies the velocity boundary conditions.

Figure 3.5 shows the imaginary parts of the velocity versus the radius at $r = 0$ on the interface at $z = 0$ for different frequency values. Similar to the real parts, the imaginary parts of the velocities in the regions $z < 0$ and $z > 0$ match exactly at the interface, confirming the continuity of velocity conditions. This consistency further supports the accuracy of the truncated solution and the robustness of the applied numerical approach.

The behavior of the velocity components reflects the physical nature of the scattering process. The real part of the velocity corresponds to the instantaneous displacement of the fluid particles, while the imaginary part captures the phase lag introduced by the scattering mechanism. As the frequency increases, the velocity components exhibit more complex patterns due to the increased influence of higher-order modes. This behavior indicates stronger interaction between the incident wave and the duct boundaries, resulting in enhanced scattering effects.

The consistent agreement of both the real and imaginary parts of the pressure and velocity across the interface reinforces the accuracy of the numerical solution and

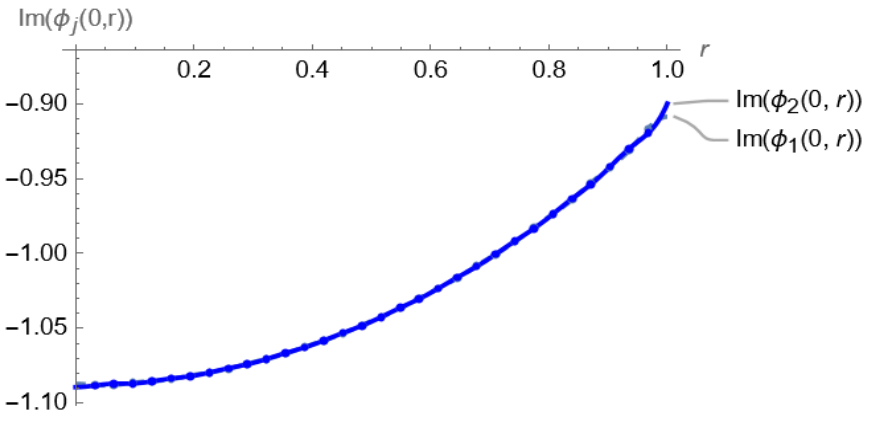

(a) $f = 50$ Hz

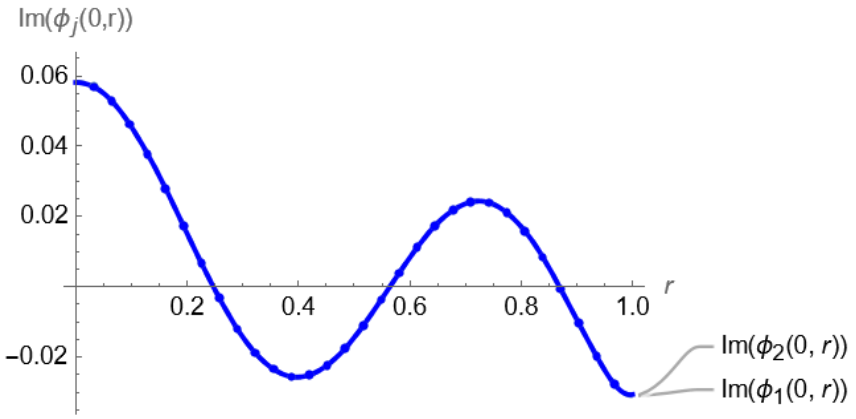

(b) $f = 500$ Hz

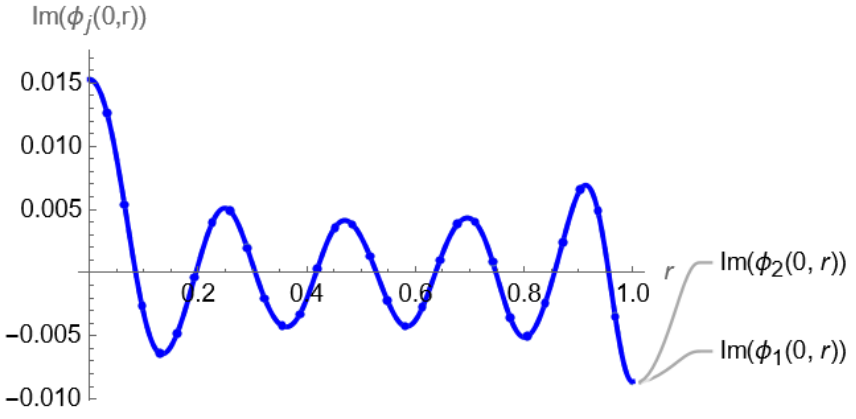

(c) $f = 1500$ Hz

FIGURE 3.3: Imaginary parts of pressures versus radius r at interface $z = 0$, where $\mu = 1$ and $a = 1$.

the effectiveness of the truncation strategy.

The ability to satisfy both pressure and velocity continuity conditions at various frequencies demonstrates the robustness of the proposed approach in analyzing scattering phenomena in ducted systems.

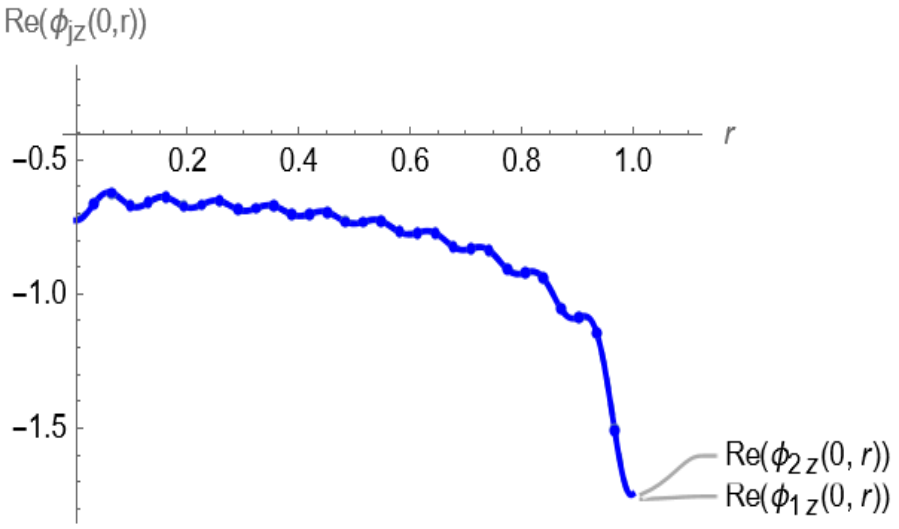

(a) $f = 50$ Hz

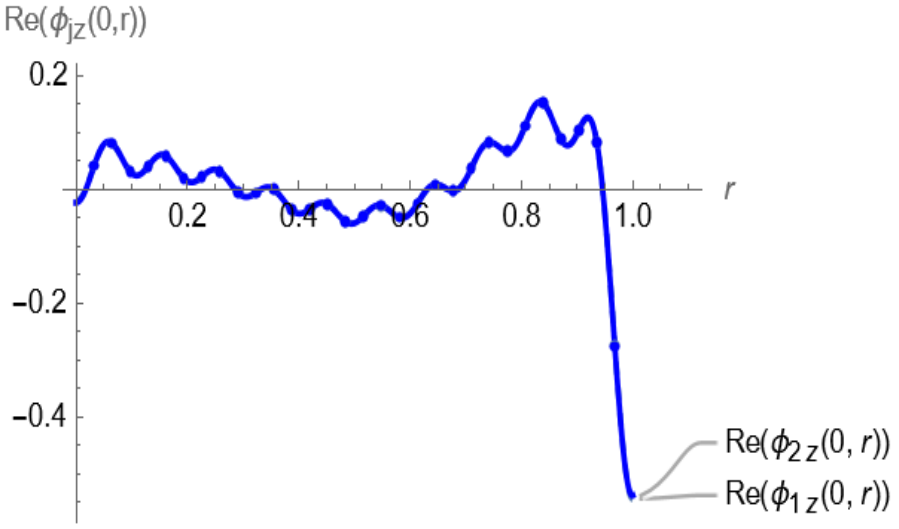

(b) $f = 500$ Hz

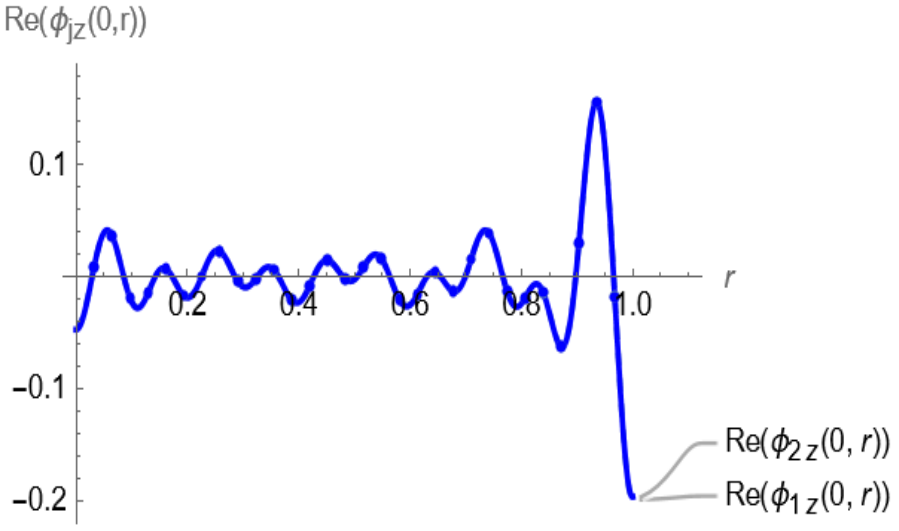

(c) $f = 1500$ Hz

FIGURE 3.4: Real parts of normal velocities versus radius r at interface $z = 0$, where $\mu = 1$ and $a = 1$.

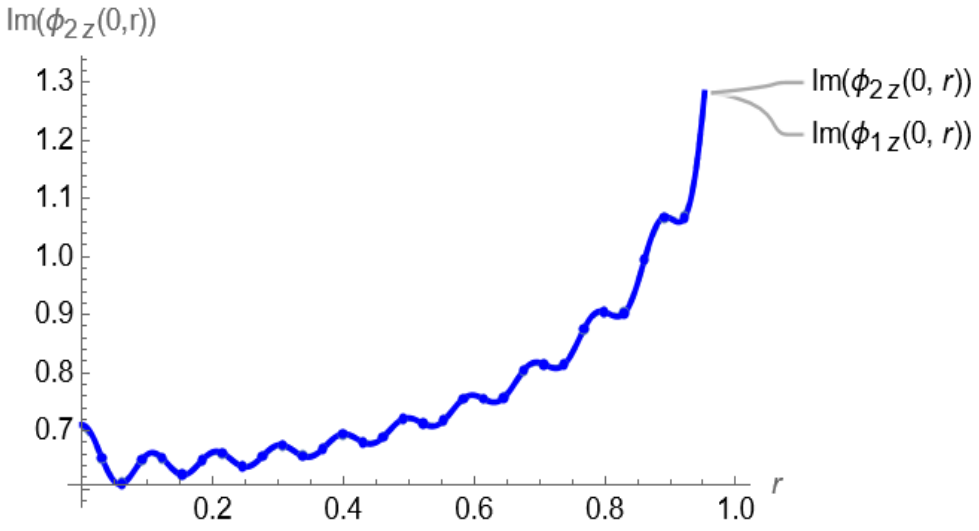

(a) $f = 50$ Hz

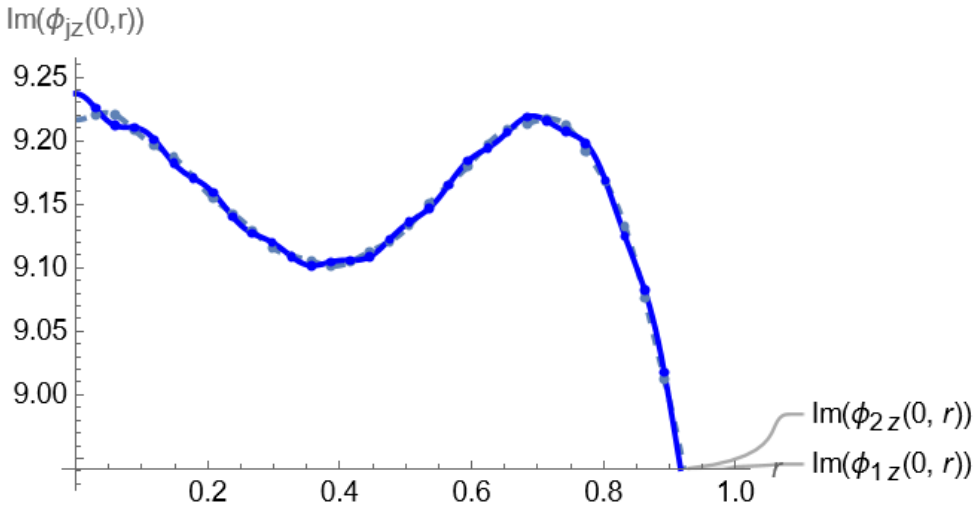

(b) $f = 500$ Hz

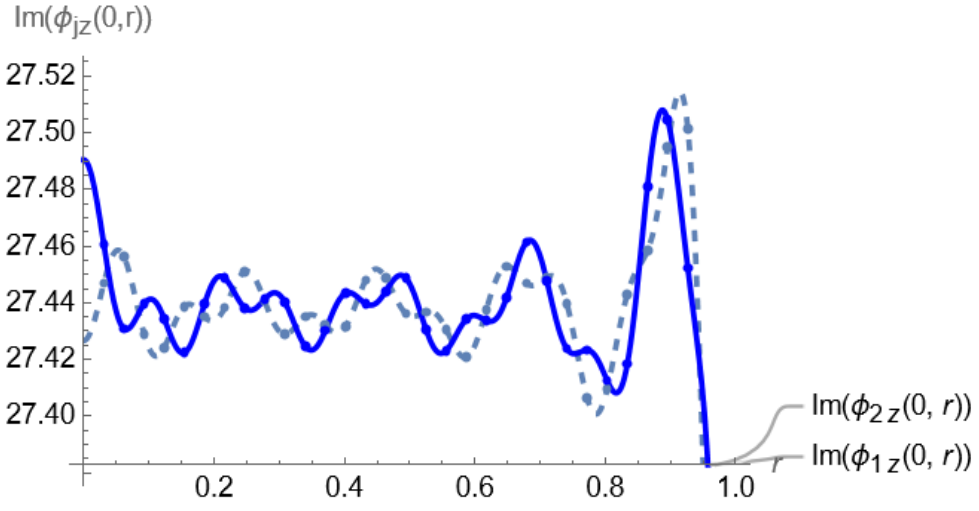

(c) $f = 1500$ Hz

FIGURE 3.5: Imaginary parts of normal velocities versus radius r at interface $z = 0$, where $\mu = 1$ and $a = 1$.

Chapter 4

The Extended Mode-Matching Method for a General Impedance Condition with Closed Ends

This chapter content regarding mode-matching solutions and exceptional points. Second, it examines solutions for symmetric configurations with both rigid and soft boundary conditions. Third, it presents enhanced solutions for antisymmetric cases that incorporate these boundary conditions. The chapter ends with a thorough analysis of numerical results, offering important insights into how the system behaves.

4.1 The Problem Having Rigid Closed End

Consider wave propagation in a waveguide rigid duct at $z = 0$, while the surface of waveguide at $z < -\ell$ is rigid. The surface of region between $-\ell < z < 0$ contains the general impedance condition. The inside of the waveguide contains compressible fluid. The physical configuration is shown in figure 4.1.
For the acoustic response the Helmholtz equation is:

$$\left\{\frac{\partial^2}{\partial r^2} + \frac{1}{r}\frac{\partial}{\partial r} + \frac{\partial^2}{\partial z^2} + k^2\right\}\varphi_j^s(r,z) = 0, \quad j = 1,2 \tag{4.1}$$

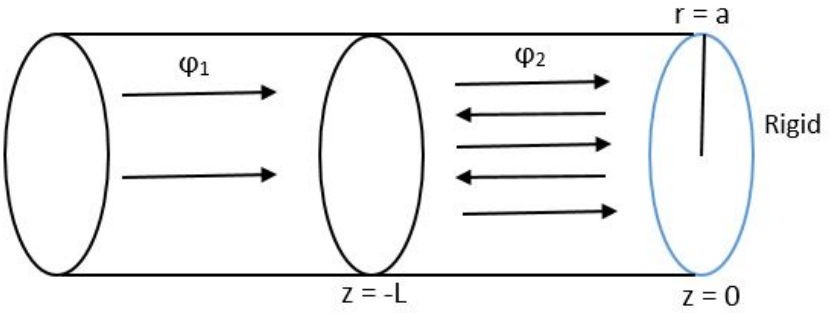

FIGURE 4.1: Diagram of the model problem with rigid condition

where the fluid potentials φ_1^s and φ_2^s express the response in the duct regions at $z < -\ell$ and $z > -\ell$, respectively. These satisfy the following rigid and impedance conditions

$$\frac{\partial \varphi_1^s}{\partial r} = 0, \quad r = a, \tag{4.2}$$

$$\frac{\partial \varphi_2^s}{\partial r} + \mu \varphi_2^s = 0, \quad r = a. \tag{4.3}$$

Following the procedure given in Chapter 3, the eigenfunction expansion of φ_1^s and φ_2^s are given below

$$\varphi_1^s(r, z) = e^{ik(z+\ell)} + \sum_{n=0}^{\infty} A_n R_{1n}(r) e^{-i\eta_n(z+\ell)}. \tag{4.4}$$

and

$$\varphi_2^s = \sum_{n}^{\infty} B_n R_{2n} e^{is_n z} + \sum_{n}^{\infty} C_n R_{2n} e^{-is_n z}. \tag{4.5}$$

The rigid conditions at $z = 0$, can be written as:

$$\frac{\partial \varphi_2^s}{\partial z} = 0, \quad z = 0, \tag{4.6}$$

and this yields $C_n = B_n$ which on substituting into (4.5), we get

$$\varphi_2^s = \sum_{n}^{\infty} B_n R_{2n} e^{is_n z} + \sum_{n}^{\infty} B_n R_{2n} e^{-is_n z}. \tag{4.7}$$

or

$$\varphi_2^s = \sum_{n}^{\infty} B_n R_{2n} [e^{is_n z} + e^{-is_n z}], \tag{4.8}$$

or

$$\varphi_2^s(r,z) = 2\sum_{n=0}^{\infty} B_n R_{2n}(r) cos(s_n z). \tag{4.9}$$

Where (φ_1^s) and (φ_2^s) are used to solve the equation in the following subsection. Therefore, for the symmetric problem the unknowns as A_n and B_n, that can be found by following the mode-matching method. The continuity of pressures at $z = -\ell$ is

$$\varphi_1^s(r,-\ell) = \varphi_2^s(r,-\ell). \tag{4.10}$$

Using (4.4) and (4.9) into (4.10), we obtain:

$$1 + \sum_{n=0}^{\infty} A_n R_{1n}(r) = 2\sum_{n=0}^{\infty} B_n R_{2n}(r)\cos(s_n\ell). \tag{4.11}$$

Multiplying both sides of (4.11) with $(rR_{1m}(r))$ and then integrating from $0 < r < a$, we get:

$$\begin{aligned}\int_0^a R_{1m}(r) r\mathrm{d}r + \sum_{n=0}^{\infty} A_n \int_0^a R_{1n}(r)R_{1m}(r) r\mathrm{d}r \\ = 2\sum_{n=0}^{\infty} B_n \cos(s_n\ell)\int_0^a R_{2n}(r)R_{1m}(r) r\mathrm{d}r.\end{aligned} \tag{4.12}$$

Using the associated orthogonality realtion into (4.12), we arrive at:

$$\delta_{0m}F_m + \sum_{n=0}^{\infty} A_n \delta_{nm} F_m = 2\sum_{n=0}^{\infty} B_n M_{mn}\cos(s_n\ell), \tag{4.13}$$

where we have used for $\delta_{0m}F_m$ and M_{nm} as:

$$\delta_{0m}F_m = \int_0^a R_{1m}(r)\mathrm{d}r, \tag{4.14}$$

$$\delta_{mn}F_m = \int_0^a R_{1n}(r) r R_{1m}(r)\mathrm{d}r, \tag{4.15}$$

and

$$M_{mn} = \int_0^a r R_{2n}(r) R_{1m}(r)\mathrm{d}r. \tag{4.16}$$

The value of the amplitude A_m is given as follows:

$$A_m F_m = -\delta_{0m} F_m + 2\sum_{n=0}^{\infty} B_n M_{mn} \cos(s_n \ell), \tag{4.17}$$

$$A_m = -\delta_{0m} + \frac{2}{F_m}\sum_{n=0}^{a} B_n M_{mn} \cos(s_n \ell). \tag{4.18}$$

Applying the continuity conditions on the normal velocities,

$$\varphi^s_{2z}(r, -\ell) = \varphi^s_{1z}(r, -\ell). \tag{4.19}$$

Using (4.4) and (4.9) into (4.19), we get:

$$e^{ik(z+\ell)} + \sum_{n=0}^{\infty} A_n R_{1n}(r) e^{-i\eta_n(z+\ell)} = 2\sum_{n=0}^{\infty} B_n R_{2n}(r) \cos(s_n z). \tag{4.20}$$

Taking the derivative of (4.20) and with respect to z, we obtain:

$$-2\sum_{n=0}^{\infty} s_n B_n R_{2n}(r) \sin(s_n z) = ike^{ikz} - \sum_{n=0}^{\infty} A_n i\eta_n R_{1n}(r) e^{-i\eta_n z}. \tag{4.21}$$

Substituting $z = -\ell$ into (4.21), gives

$$2\sum_{n=0}^{\infty} s_n B_n R_{2n}(r) \sin(s_n \ell) = ik - \sum_{n=0}^{\infty} A_n i\eta_n R_{1n}(r). \tag{4.22}$$

Multiplying (4.22) with ($rR_{2m}(r)$) and then integrating from $0 < r < a$,

$$\begin{aligned} 2\sum_{n=0}^{\infty} B_n \sin(s_n \ell) \int_0^a rR_{2n}(r)R_{2m}(r)\mathrm{d}r = ik \int_0^a R_{2m}(r)\mathrm{d}r \\ - \sum_{n=0}^{\infty} A_n i\eta_n \int_0^a rR_{1n}(r)R_{2m}(r)\mathrm{d}r. \end{aligned} \tag{4.23}$$

Applying the orthogonality relation, we obtain:

$$2B_m \sin(s_m \ell)\delta_{mn} F_m = ikM_{0m} - \sum_{n=0}^{\infty} iA_n \eta_n P_{mn}. \tag{4.24}$$

Here, we provide the explicit expressions for $\delta_{nm}F_m$, M_{0m}, and P_{nm}

$$\delta_{mn}F_m = \int_0^a rR_{2n}(r)R_{2m}(r)\mathrm{d}r, \tag{4.25}$$

$$M_{0m} = \int_0^a rR_{2m}(r)\mathrm{d}r, \tag{4.26}$$

and

$$P_{mn} = \int_0^a rR_{1n}(r)R_{2m}(r)\mathrm{d}r. \tag{4.27}$$

After that, the resulting equation becomes:

$$B_m = \frac{ikM_{0m}}{2s_m \sin(s_m\ell)} - \frac{i}{2s_m \sin(s_m\ell)F_m}\sum_{n=0}^{\infty} A_n\eta_n P_{mn}. \tag{4.28}$$

4.1.1 Extended Mode-Matching Conditions for Rigid Closed End

We enhance the mode-matching solution for exceptional point. In the context of wave propagation, an exceptional point refers to a point in space where the wave exhibits unusual behavior. Specifically, s_1 is a singular point where the wave behavior changes abruptly. Exceptional points, such as s_1, play a crucial role in understanding various wave phenomena, including wave scattering and nonlinear wave dynamics. Considering the exceptional point at s_1, on equation 3.54 gives

$$\begin{aligned}\varphi^s_{EP_2} = \bar{B}_1 &\left[-\frac{s_1}{\tau_1^2}\chi(r,\tau) + izR_{2n}(r)\right] e^{is_1 z} \\ + C_1 &\left[-\frac{s_1}{\tau_1^2}\chi(r,\tau) - izR_{2n}(r)\right] e^{-is_1 z}.\end{aligned} \tag{4.29}$$

This implies that the coefficients C_1 and B_1 are equal, which is a necessary condition for symmetry in certain mathematical equations. By putting $C = B$ into (4.29), we obtain:

$$\begin{aligned}\varphi^s_{EP2} = \bar{B}_1 &\left[-\frac{s_1}{\tau_1^2}\chi(r,\tau) + izR_{2n}(r)]e^{is_1 z}\right] \\ + \bar{B}_1 &\left[-\frac{s_1}{\tau_1^2}\chi(r,\tau) - izR_{2n}(r)]e^{-is_1 z}\right].\end{aligned} \tag{4.30}$$

The value of $\cos(s_1 z)$ and $\sin(s_1 z)$ is given hence

$$\cos(s_1 z) = \frac{e^{is_1 z} + e^{-is_1 z}}{2}, \tag{4.31}$$

and

$$\sin(s_1 z) = \frac{e^{is_1 z} - e^{-is_1 z}}{2}. \tag{4.32}$$

Using the (4.31) and (4.32) into (4.30), yield

$$\begin{aligned} \varphi_2^s(r,z) &= 2\sum_{n=0}^{\infty} B_n R_{2n}(r)\cos(s_n z) \\ +\bar{B}_1^s &\left[-\frac{s_1}{\tau_1^2} 2\cos(s_1 z)\chi(r,\tau) + 2izR_{2n}(r)\sin(s_1 z)\right]. \end{aligned} \tag{4.33}$$

By incorporating these techniques, mode matching solutions can provide more accurate and reliable results, ensuring continuity of pressure and improving the overall fidelity of acoustic wave propagation simulations

$$\varphi_1^s(r,z) = \varphi_2^s(r,z). \tag{4.34}$$

Substituting $z = -\ell$ into (4.34), the following equation is obtained

$$\varphi_1^s(r,-\ell) = \varphi_2^s(r,-\ell). \tag{4.35}$$

Using (4.4) and (4.33) into (4.35), we get:

$$\begin{aligned} e^{ik(z+\ell)} &+ \sum_{n=0}^{\infty} A_n R_{1n}(r) e^{-i\eta_n(z+\ell)} \\ &= \bar{B}_1^s \left[\frac{-2s_1}{\tau_1}\cos(s_1 z)\chi(\tau_1 z) + 2izR_{2n}(\tau_1 z)\sin(s_1 z)\right]. \end{aligned} \tag{4.36}$$

Using (φ_2^s) into (4.36) equation become:

$$\begin{aligned} e^{ik(z+\ell)} + \sum_{n=0}^{\infty} A_n R_{1n}(r) e^{-i\eta_n(z+\ell)} &= 2\sum_{n=0}^{\infty} B_n R_{2n}(r)\cos(s_n z) \\ &+ \bar{B}_1^s \left[\frac{-2s_1}{\tau_1}\cos(s_1 z)\chi(\tau_1 z) + 2ziR_{2n}(\tau_1 z)\sin(s_1 z)\right]. \end{aligned} \tag{4.37}$$

Putting $z = -\ell$ into (4.37), after simplification we get:

$$1 + \sum_{n=0}^{\infty} A_n R_{1n}(r) = 2\sum_{n=0}^{\infty} B_n R_{2n}(r)\cos(s_n\ell) + \bar{B}_1^s\left[\frac{-2s_1}{\tau_1}\cos(s_1 z)\chi(\tau_1, r) + 2i\ell R_{2n}(\tau_1, r)\sin(s_1\ell)\right]. \tag{4.38}$$

Multiplying (4.38) with ($rR_{1m}(r)$) and then integrating from $0 < r < a$,

$$\int_0^a rR_{1m}(r)\mathrm{d}r + \sum_{n=0}^{\infty} A_n \int_0^a rR_{1n}(r)R_{1m}(r)\mathrm{d}r = 2\sum_{n=0}^{\infty} B_n\cos(s_n\ell)\int_0^a rR_{2n}(r)R_{1m}(r)\mathrm{d}r + \bar{B}_1^s\left[\frac{-2s_1}{\tau_1}\cos(s_1 z)\int_0^a \chi(\tau_1, r)R_{1m}(r)\mathrm{d}r + 2i\ell\sin(s_1\ell)\int_0^a R_{1n}(r)R_{1m}(r)\mathrm{d}r\right]. \tag{4.39}$$

Simplifying the (4.39) yields:

$$A_m = -\delta_{0m} + \frac{2}{F_m}\sum_{n=0}^{a} B_n M_{mn}\cos(s_n\ell) + \frac{\bar{B}_1^s}{F_m}\left[\frac{-2s_1}{\tau_1}\cos(s_1 z)M_{1m} + 2i\ell\sin(s_1\ell)M_{mn}\right]. \tag{4.40}$$

Orthogonality relation can be express as:

$$\delta_{nm}F_m = \int_0^a rR_{1n}(r)R_{1m}(r)\mathrm{d}r. \tag{4.41}$$

The explicit expressions for δ_{0m}, M_{0m}, and M_{1m} are provided below

$$\delta_{0m} = \int_0^a rR_{1m}(r)\mathrm{d}r, \tag{4.42}$$

$$M_{1m} = \int_0^a \chi(\tau_1, r)rR_{1m}(r)\mathrm{d}r, \tag{4.43}$$

$$M_{nm} = \int_0^a r R_{1n}(r) R_{1m}(r) \mathrm{d}r. \tag{4.44}$$

The continuity condition of normal velocities can be expressed as:

$$\varphi^s_{2z}(r,-z) = \varphi^s_{1z}(r,-z). \tag{4.45}$$

Putting (4.2) and (4.33) into (4.45) we get:

$$e^{ik(z+\ell)} + \sum_{n=0}^{\infty} A_n R_{1n}(r) e^{-i\eta_n(z+\ell)} = 2\sum_{n=0}^{\infty} B_n R_{2n}(r)\cos(s_n z) + \bar{B}^s_1 \left[\frac{-2s_1}{\tau_1}\cos(s_1 z)\chi(\tau_1, r) + 2izR_{2n}(\tau_1, r)\sin(s_1 z)\right]. \tag{4.46}$$

Taking the derivative of (4.46) with respect to z, yields:

$$ike^{ik(z+\ell)} - i\sum_{n=0}^{\infty} \eta_n A_n R_{1n}(r) e^{-i\eta_n(z+\ell)} = -2\sum_{n=0}^{\infty} s_n B_n R_{2n}(r)\sin(s_n z) + \bar{B}^s_1 \left[\frac{2s_1^2}{\tau_1^2}\sin(s_1 z)\chi(\tau_1 z) + 2iR_{2n}(r)\sin(s_1 z) + 2\iota z s_1 cos(s_1 z) R_{2n}(r)\right]. \tag{4.47}$$

Using $z = -\ell$ into (4.47) we obtain:

$$2\sum_{n=0}^{\infty} B_n s_n R_{2n}(r)\sin(s_n \ell) = ik - i\sum_{n=0}^{\infty} A_n \eta_n R_{1n}(r) + \bar{B}^s_1 \left[2\frac{s_1^2}{\tau_1^2}\sin(s_1\ell)\chi(\tau_1, r) - 2i\sin(s_1\ell)R_{2n}(r) - 2i\ell s_1\cos(s_1\ell)R_{2n}(r)\right]. \tag{4.48}$$

Multiplying (4.48) with ($rR_{2m}(r)$), and then integrating from ($0 < r < a$),

$$\bar{B}^s_1 \left[2\frac{s_1^2}{\tau_1^2}\sin(s_1\ell)\int_0^a r R_{2m}(r)\chi(\tau_1, r)\mathrm{d}r - 2i\sin(s_1\ell)\int_0^a r R_{2m}(r)R_{2n}(r)\mathrm{d}r\right]$$

$$- \bar{B}^s_1 \left[2i_1\cos(s_1\ell)\int_0^a r R_{2n}(r)R_{2m}(r)\mathrm{d}r\right] + 2\sum_{n=0}^{\infty} B_n s_n \sin(s_n\ell)\int_0^a r R_{2n}(r)R_{2m}(r)\mathrm{d}r = ik\int_0^a R_{2m}(r)\mathrm{d}r - \sum_{n=0}^{\infty} A_n i\eta_n \int_0^a r R_{1n}(r)R_{2m}(r)\mathrm{d}r. \tag{4.49}$$

After the simplification of (4.49) we get:

$$\bar{B_1^s}\left[2\frac{s_1^2}{\tau_1^2}\sin(s_1\ell)H\right] - \bar{B_1^s}T + 2B_1 s_1 \sin(s_1\ell)Q = ikM_{0m} - i\sum_{n=0}^{\infty} A_n\eta_n P_{nm} \quad (4.50)$$

Upon simplification of (4.49), the resulting equation is:

$$\begin{aligned} B_m = {} & \frac{ikM_{0m}}{2s_m\sin(s_m\ell)} - \frac{i}{2s_m\sin(s_m\ell)F_m}\sum_{n=0}^{\infty} A_n\eta_n P_{nm} \\ & + \frac{\bar{B_1^s}}{2s_m\sin(s_m\ell)F_m}\left[2\frac{s_1^2}{\tau_1^2}\sin(s_1L)H_{nm} + 2i\sin(s_1\ell)T_{nm} - 2iLs_1\cos(s_1\ell)N_{nm}\right]. \end{aligned} \quad (4.51)$$

Orthogonality relation can be express as:

$$\delta_{nm}F_m = \int_0^a rR_{1n}(r)R_{1m}(r)\mathrm{d}r, \quad (4.52)$$

The values of M_{0m} and P_{nm} are expressed as:

$$M_{0m} = \int_0^a rR_{2m}(r)\mathrm{d}r, \quad (4.53)$$

$$P_{nm} = \int_0^a rR_{1n}(r)R_{2m}(r)\mathrm{d}r. \quad (4.54)$$

Multiplying (4.48) with ($\chi(\tau_1, r)$) and then integrating from $0 < r < a$,

$$\begin{aligned} & B_1^s\left[-\frac{s_1^2}{\tau_1^2}\cos(s_1\ell)\int_0^a \chi^2(\tau_1,r)r\mathrm{d}r - i\cos(s_1\ell)\int_0^a r\chi_(\tau_1,r)R_{2n}(r)\mathrm{d}r\right] \\ & + B_1^s\left[i_1\sin(s_1\ell)\int_0^a rR_{2n}(r)\chi(\tau_1,r)\mathrm{d}r\right] + \sum_{n=0}^{\infty} B_n\sin(s_n\ell)s_n\int_0^a r\chi(\tau_1,r)R_{2n}(r)\mathrm{d}r \\ & = \frac{ik}{2}\int_0^a r\chi(\tau_1,r)\mathrm{d}r - \frac{1}{2}i\sum_{n=0}^{\infty} A_n\eta_n\int_0^a R_{1n}(r)\chi(\tau_1,r)\mathrm{d}r. \end{aligned} \quad (4.55)$$

After the simplification of (4.55) we get:

$$\begin{aligned} & B_1^s 2\frac{s_1^2}{\tau_1^2}\sin(s_1\ell)Q + 2i\sin(s_1\ell)B_1^s T - B_1^s 2is_1\ell\sin(s_1\ell)H + B_1 2is_1\sin(s_1\ell)M \\ & = ik\ell_{0m} - i\sum_{n=0}^{\infty} A_n\eta_n M_{1n}. \end{aligned} \quad (4.56)$$

The parameters Q, H, M, L_{0m}, and M_{1n} are defined as:

$$Q = \int_0^a r\chi^2(\tau_1, r)\mathrm{d}r, \tag{4.57}$$

$$H = \int_0^a rR_{2n}(r)\chi(\tau_1, r)\mathrm{d}r, \tag{4.58}$$

$$L_{01} = \int_0^a r\chi(\tau_1, r)\mathrm{d}r, \tag{4.59}$$

and

$$V_{0n} = \int_0^a rR_{1n}(r)\chi(\tau_1, r)\mathrm{d}r. \tag{4.60}$$

The coefficient of the variable are the elements of the matrix which define the linear transformation. A linear transformation is a function between vector that preserves the operation of vector addition and scalar multiplication. By representing coefficients as matrices, we can leverage the power of linear algebra to solve systems of linear equation and perform various other operation

$$\begin{bmatrix} 2s_1\sin(s_1\ell)Q & 2\frac{s_1^2}{\tau_1^2}\sin(s_1\ell)H - T \\ 0 & 2\frac{s_1^2}{\tau_1^2}\sin(s_1\ell)N \end{bmatrix} \begin{bmatrix} B^s \\ \bar{B}_1^s \end{bmatrix} = \begin{bmatrix} iKM_{0m} - i\sum_{n=0}^{\infty} A_n\eta_n P_{nm} \\ iK\ell_{01} - i\sum_{n=0}^{\infty} A_n\eta_n V_{0n} \end{bmatrix}. \tag{4.61}$$

4.2 Numerical Results

This section presents a numerical analysis of the solution obtained at the previous section for the rigid interface. The system is truncated using $n = 15$ terms, ensuring that the solution captures the key modes while maintaining computational efficiency. The analysis is conducted using the following parameter values: duct radius $a = 1\,\mathrm{cm}$, interface height $h = 1\,\mathrm{cm}$, viscosity coefficient $\mu = 1$, length $\ell = 0.5\,\mathrm{cm}$, speed of sound in air $c = 343.5\,\mathrm{m/s}$, and air density $\rho = 1.2$.

Figure 4.2 illustrates the real and imaginary parts of the pressure for the symmetric problem as a function of the radius at $r = 0$ on the interface at $z = -\ell$. It is clearly seen that the real parts of the pressure in the regions $z < -\ell$ and $z > -\ell$ coincide perfectly at the interface. Similarly, the imaginary parts of the pressure in these

regions also align exactly at the interface, consistent with the continuity condition of pressure. This consistency verifies the accuracy of the truncated solution and confirms the robustness and reliability of the numerical approach across different frequency conditions. Figure 4.3 illustrates the real and imaginary parts of the

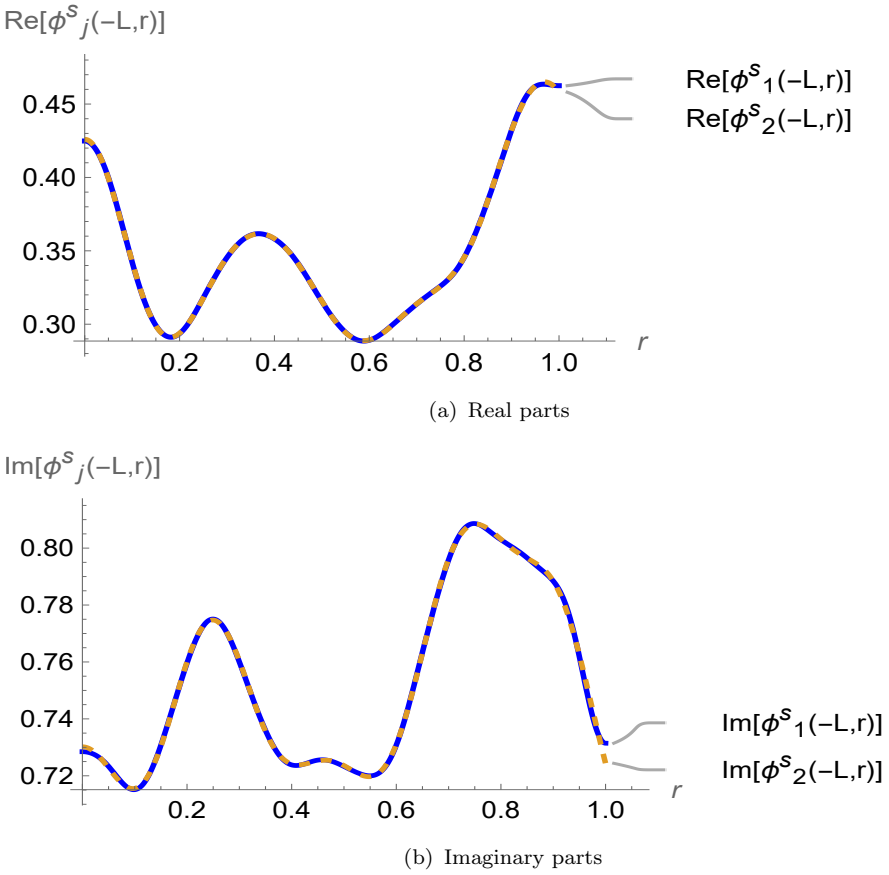

(a) Real parts

(b) Imaginary parts

FIGURE 4.2: With rigid closed end: The real and imaginary parts of pressures versus radius r at interface $z = -\ell$, where $\mu = 1$, $\ell = 0.5$ and $a = 1$.

normal velocity for the symmetric problem as a function of the radius at $r = 0$ on the interface at $z = -\ell$.

It is evident that the real parts of the normal velocity in the regions $z < -\ell$ and $z > -\ell$ match precisely at the interface.

Likewise, the imaginary parts of the normal velocity in these regions also align exactly at the interface,

which satisfies the continuity condition for normal velocity.

This agreement confirms the accuracy of the truncated solution and demonstrates the robustness and reliability of the numerical method under varying frequency conditions.

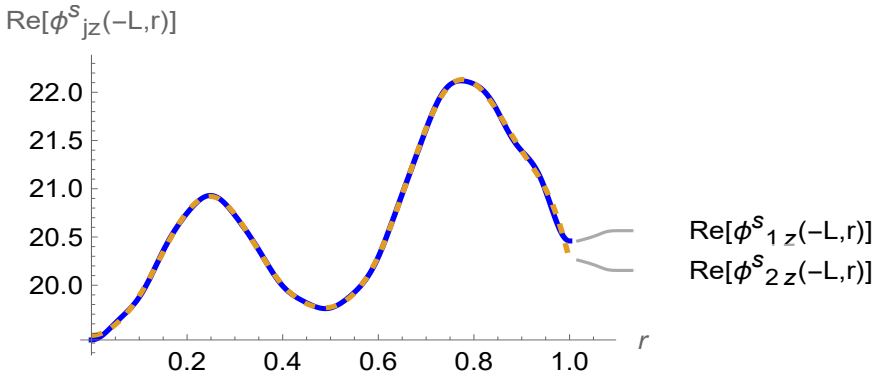

(a) Real parts

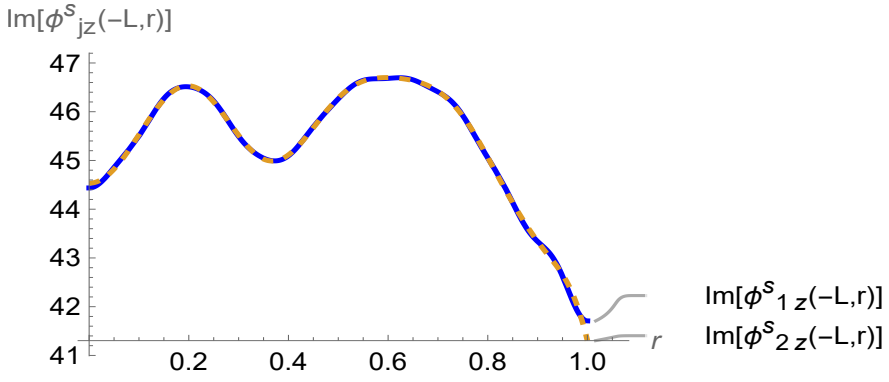

(b) Imaginary parts

FIGURE 4.3: With rigid closed end: The real and imaginary parts of normal velocities versus radius r at interface $z = -\ell$, where $\mu = 1$, $\ell = 0.5$ and $a = 1$.

4.3 The Problem Having Soft Closed End

Consider wave propagation in a waveguide soft disc at $z = 0$, while the surface at of waveguide at $z < -L$ is rigid. The surface of region between $-L < z < 0$ contains the general impedance condition. The inside of the waveguide contains compressible fluid. The physical configuration is as shown in Fig. 4.4.

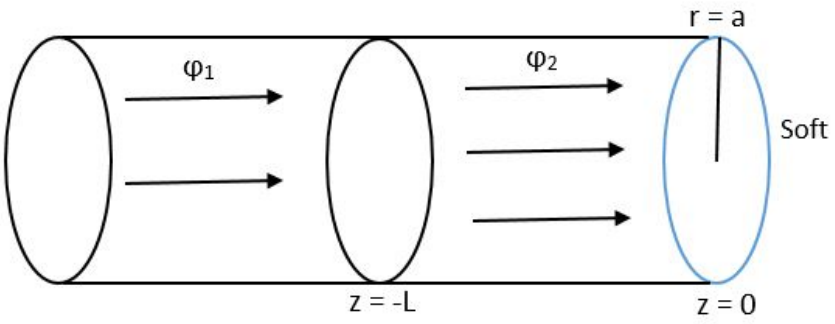

FIGURE 4.4: Diagram of the model problem

The govening equations are same Helmholts equation, rigid condition and impedance condition.

On the condition at $z = 0$ is soft that is

$$\varphi_2(r, z) = 0. \tag{4.62}$$

4.3.1 Standrad Mode-Matching Solution

Following the procedure given in chapter 3, the eigenfunction expansion of φ_1^a and φ_2^a are given below

$$\varphi_1^a(r, z) = e^{ik(z+\ell)} + \sum_{n=0}^{\infty} A_n R_{1n}(r) e^{-i\eta_n(z+\ell)}, \tag{4.63}$$

and

$$\varphi_2^a = \sum_{n}^{\infty} B_n R_{2n} e^{is_n z} + \sum_{n}^{\infty} C_n R_{2n} e^{-is_n z}. \tag{4.64}$$

The soft condition at $z = 0$ yields $C_n = -B_n$ which on substituting into (4.64), we get:

$$\varphi_2^a(r, z) = 2i \sum_{n=0}^{\infty} B_n R_{2n}(r) \sin(s_n z). \tag{4.65}$$

The problem yields anti-symmetric modes, and to find the unknown amplitudes, the continuity condition is

$$\varphi_1^a(r, -\ell) = \varphi_2^a(r, -\ell). \tag{4.66}$$

Using the fields into the continuity conditions, we get:

$$1 + \sum_{n=0}^{\infty} A_n R_{1n}(r) = -2 \sum_{n=0}^{\infty} B_n R_{2n}(r) \sin(s_n \ell). \tag{4.67}$$

Multiplying (4.67) with $(R_{1m}(r)r)$ and then integrating from $0 < r < a$. Orthogonality relation can be express as:

$$\begin{aligned}\int_0^a rR_{1m}(r)\mathrm{d}r + \sum_{n=0}^{\infty} A_n \int_0^a rR_{1n}(r)R_{1m}(r)\mathrm{d}r \\ = 2\sum_{n=0}^{\infty} B_n \sin(s_n\ell)\int_0^a R_{2n}(r)R_{1m}(r)r\mathrm{d}r.\end{aligned} \tag{4.68}$$

simplification leads to

$$\delta_{0m}F_m + \sum_{n=0}^{\infty} A_n\delta_{nm}F_m = -2\sum_{n=0}^{\infty} B_n M_{mn}\sin(s_n\ell), \tag{4.69}$$

where, we define the values of M_{nm} and $\delta_{0m}F_m$ as follows:

$$\delta_{nm}F_m = \int_0^a rR_{1n}(r)R_{1m}(r)\mathrm{d}r, \tag{4.70}$$

and

$$M_{nm} = \int_0^a R_{2n}(r)R_{1m}(r)\mathrm{d}r. \tag{4.71}$$

from (4.70) leads to

$$A_m = -\delta_{0m} - \frac{2}{F_m}\sum_{n=0}^{\infty} B_n M_{mn}\sin(s_n\ell). \tag{4.72}$$

In antisymmetric configurations, the continuity of normal velocity can be explained as follows.

The normal velocity component is the velocity component perpendicular to the interface between two media.

In an antisymmetric configuration, the normal velocity component must be continuous across the interface

$$\varphi_{2z}^a(r,-\ell) = \varphi_{1z}^a(r,-\ell). \tag{4.73}$$

Putting the field into the velocity condition at $z = -\ell$ we get:

$$2i\sum_{n=0}^{\infty} B_n R_{2n}(r)s_n\cos(s_n\ell) = ik - \sum_{n=0}^{\infty} A_n i\eta_n R_{1n}(r). \tag{4.74}$$

Multiplying (4.74) by $rR_{2m}(r)$ and then integrating over the interval $0 < r < a$, to obtain:

$$2\sum_{n=0}^{\infty} B_n s_n \cos(s_n \ell) \int_0^a rR_{2n}(r)R_{2m}(r)\mathrm{d}r = k\int_0^a rR_{2m}(r)\mathrm{d}r - \sum_{n=0}^{\infty} A_n \eta_n \int_0^a rR_{1n}(r)R_{2m}(r)\mathrm{d}r. \tag{4.75}$$

Orthogonality relation express as:

$$2B_n s_n \cos(s_n \ell)\delta_{mn} F_m = kP_{0m} - \sum_{n=0}^{\infty} A_n \eta_n M_{mn}, \tag{4.76}$$

leads to

$$B_m = \frac{kP_{0m}}{2is_m \cos(s_m \ell)} - \frac{1}{2\cos(s_m \ell)F_m} \sum_{n=0}^{\infty} A_n \eta_n M_{mn}. \tag{4.77}$$

We express the value of P_{0m} and M_{nm} as:

$$P_{0m} = \int_0^a rR_{2m}(r)\mathrm{d}r, \tag{4.78}$$

and

$$M_{nm} = \int_0^a rR_{1n}(r)R_{2m}(r)\mathrm{d}r, \tag{4.79}$$

orthogonality relation is express as:

$$\delta_{nm} F_m = \int_0^a rR_{2n}(r)R_{2m}(r)\mathrm{d}r.. \tag{4.80}$$

4.3.2 Extended Mode-Matching Conditions for Soft Closed End

For antisymmetric case, substituting $C_1 = -B_1$ into (4.33) yield

$$\varphi_2^a(r,z) = 2i\sum_{n=0}^{\infty} B_n R_{2n}(r)\sin(s_n z) + \bar{B}_1^a \left[\frac{2s_1}{\tau_1^2}\sin(s_1 z)\chi(\tau_1 r) + 2izR_{2n}\cos(s_1 z)\right]. \tag{4.81}$$

The continuity of pressure condition

$$\varphi_1^a(r,-\ell) = \varphi_2^a(r,-\ell). \tag{4.82}$$

Using (4.4) and (4.81) into (4.82), we obtain:

$$\begin{aligned} e^{ik(z+\ell)} + \sum_{n=0}^{\infty} A_n R_{1n}(r) e^{i\eta_n(z+\ell)} \\ = B_1^a \left[-\frac{2s_1^2}{\tau_1^2}\chi(\tau_1, r) sin(s_1 z) + 2iR_{2n}(r)\cos(s_1 z) + 2izR_{2n}(r)\cos(s_1 z) \right] \\ +2i\sum_{n=0}^{\infty} B_n R_{2n}(r)\sin(s_n z). \end{aligned} \tag{4.83}$$

Using $z = -\ell$ into the equation (4.83),yield to

$$\begin{aligned} 1 + \sum_{n=0}^{\infty} A_n R_{1n}(r) = -2\sum_{n=0}^{\infty} B_n R_{2n}(r)\sin(s_n \ell) \\ +\bar{B}_1^s \left[\frac{-2s_1}{\tau_1}\sin(s_1\ell)\chi(\tau_1 r) + 2_{2n}(\tau_1 r)\cos(s_1\ell) \right]. \end{aligned} \tag{4.84}$$

Multiplying (4.84) with ($rR_{1m}(r)$) and then integrating over the interval $0 < r < a$,

we obtain:

$$\begin{aligned} \int_0^a rR_{1m}(r)\mathrm{dr} + \sum_{n=0}^{\infty} A_n \int_0^a rR_{1n}(r)R_{1m}(r)\mathrm{dr} \\ = -2\sum_{n=0}^{\infty} B_n \sin(s_n\ell)\int_0^a rR_{2n}(r)R_{1m}(r)\mathrm{dr} \\ + \bar{B}_1^s \left[\frac{-2s_1}{\tau_1}\sin(s_1 z)\int_0^a \chi(\tau_1 r)R_{1m}(r)\mathrm{dr} + 2\ell\cos(s_1\ell)\int_0^a R_{1n}(r)R_{1m}(r)\mathrm{dr} \right]. \end{aligned} \tag{4.85}$$

Simplification leads to

$$\begin{aligned} A_m = -\delta_{0m} - \frac{2}{F_m}\sum_{n=0}^{a} B_n M_{mn}\sin(s_n\ell) \\ + \frac{\bar{B}_1^s}{F_m}\left[\frac{-2s_1}{\tau_1}\sin(s_1 z)M_{1m} + 2\ell\cos(s_1\ell)M_{mn} \right]. \end{aligned} \tag{4.86}$$

The continuity of normal velocity condition given below

$$\varphi^a_{2z}(r,-z) = \varphi^a_{1z}(r,-z) \tag{4.87}$$

Using (4.4) and (4.81) into (4.88), we get:

$$\begin{aligned} &ike^{ik(z+\ell)} - i\sum_{n=0}^{\infty}\eta_n A_n R_{1n}(r)e^{-i\eta_n(z+\ell)} \\ &= 2i\sum_{n=0}^{\infty} s_n B_n R_{2n}(r)\cos(s_n z) + \bar{B}^a_1\left[-\frac{2s_1^2}{\tau_1^2}\cos(s_1 z)\chi(\tau_1 r) + 2iR_{2n}\cos(s_1 z) - 2iz\sin(s_n z)\right]. \end{aligned} \tag{4.88}$$

Putting $z = -\ell$ into (4.88) reduce to

$$\begin{aligned} &2i\sum_{n=0}^{\infty} B_n s_n R_{2n}(r)\cos(s_n\ell) = ik - i\sum_{n=0}^{\infty} A_n\eta_n R_{1n}(r) \\ &+ \bar{B}^s_1\left[-2\frac{s_1^2}{\tau_1^2}\cos(s_1\ell)\chi(\tau_1, r) + 2i\cos(s_1\ell)R_{2n}(r) + 2i\ell s_1\sin(s_1\ell)R_{2n}(r)\right]. \end{aligned} \tag{4.89}$$

Now, multiplying (4.89) with ($rR_{2m}(r)$) and integrating over the interval $0 < r < a$, we obtain:

$$\begin{aligned} \bar{B}^a_1\left[-\frac{s_1^2}{\tau_1^2}\sin(s_1\ell)\int_0^a rR_{2m}(r)\chi(\tau_1 r)\mathrm{d}r + i\sin(s_1\ell)\int_0^a rR_{2m}(r)R_{2n}(r)\mathrm{d}r\right] \\ - \bar{B}^s_1\left[i_1\cos(s_1\ell)\int_0^a rR_{2n}(r)R_{2m}(r)\mathrm{d}r\right] \\ + \sum_{n=0}^{\infty} B_n s_n\cos(s_n\ell)\int_0^a rR_{2n}(r)R_{2m}(r)\mathrm{d}r \\ = \frac{k}{2}\int_0^a R_{2m}(r)\mathrm{d}r - \frac{1}{2i}\sum_{n=0}^{\infty} A_n i\eta_n\int_0^a rR_{1n}(r)R_{2m}(r)\mathrm{d}r, \end{aligned} \tag{4.90}$$

which leads to

$$\begin{aligned} B_m &= \frac{kM_{0m}}{2s_m\cos(s_m\ell)} + \frac{1}{2\cos(s_m\ell)}\sum_{n=0}^{\infty} A_n\eta_n P_{nm} \\ &+ \frac{\bar{B}^a_1}{s_m i\sin(s_m\ell)}\left[-2\frac{s_1^2}{\tau_1^2}\cos(s_1\ell)Q_{nm} - i\ell s_1\sin(s_1\ell)M_{1m} + i\cos(s_1\ell)M_{2m}\right], \end{aligned} \tag{4.91}$$

where, we will discuss the above assumption by assigning some specific values

$$\delta_{0m} = \int_0^a r R_{2m}(r)\mathrm{d}r, \tag{4.92}$$

$$Q_{nm} = \int_0^a r R_{2m}(r) R_{1n}(r), \tag{4.93}$$

$$M_{1m} = \int_0^a r\chi(r,\tau) R_{2m}(r)\mathrm{d}r, \tag{4.94}$$

and

$$M_{2m} = \int_0^a R_{2n}(r) r R_{2m}\mathrm{d}r. \tag{4.95}$$

Orthogonality relation is express as:

$$F_m = \int_0^a r R_{1n}(r) R_{2m}(r)\mathrm{d}r. \tag{4.96}$$

Note: that since $\chi(\tau, r)$ is self-orthogonal. However, although it does not give information about B_1 it does provide information about $\bar{B_1}$. Where the coefficient $\bar{B_1}$ is associated with the additional functions and the overbear indicates that these occur due to the double root s_1. It is important to note that the function $\chi(r\tau)$ is needed to ensure that the eigenfunction expansion converges point-wise. Multiplying (4.89) with $\chi(\tau_1, r)r$ and then integrating over $0 < r < a$,

$$\begin{aligned}
\bar{B_1^a}\left[-\frac{s_1^2}{\tau_1^2}\cos(s_1\ell)\int_0^a r\chi^2(\tau_1,r)\mathrm{d}r + 2i\ell s_1\sin(s_1\ell)\int_a^a \chi_(\tau_1,r) r R_{2n}(r)\mathrm{d}r\right] \\
- \bar{B_1^a}\left[+2icos(s_1\ell)\int_0^a \chi_(\tau_1,r) R_{2n}(r) r\mathrm{d}r\right] \\
- \left[2i\ell\sum_{n=0}^{\infty} B_n s_n\cos(s_n\ell)s_n\int_0^a \chi(\tau_1,r) R_{2n}(r) r\mathrm{d}r\right] \\
= ik\int_0^a r\chi(\tau_1,r)\mathrm{d}r - i\sum_{n=0}^{\infty} A_n\eta_n\int_0^a \chi(\tau_1,r) R_{1n}(r) r\mathrm{d}r,
\end{aligned} \tag{4.97}$$

The equation can be rewritten as follows, which on simplification yields:

$$\begin{aligned}
-B_1^a 2\frac{s_1^2}{\tau_1^2}\cos(s_1\ell)Q + 2i\cos(s_1\ell)TB_1^a + B_2^a 2is_1\ell\sin(s_1\ell)H \\
-B_1 2is_1\cos(s_1\ell)M = ik\ell_{01} - i\sum_{n=0}^{\infty} A_n\eta_n V_{0n},
\end{aligned} \tag{4.98}$$

where, we define the value of Q,T,H,ℓ_{01} and M_{1n}

$$Q = \int_0^a r\chi^2(\tau_1, r)\mathrm{dr}, \tag{4.99}$$

$$T = \int_0^a r\chi(\tau_1, r)R_{2n}(r)\mathrm{dr}, \tag{4.100}$$

$$\ell_{01} = \int_0^a r\chi(\tau_1, r)\mathrm{dr}, \tag{4.101}$$

and

$$V_{0n} = \int_0^a r\chi(\tau_1, r)R_{1n}(r)\mathrm{dr}. \tag{4.102}$$

Create a matrix using the coefficients of the variables. The coefficients of the variable will form the rows of the matrix In a matrix notation we can write

$$\begin{bmatrix} -2is_1\cos(s_1\ell)Q & -2\frac{s_1^2}{\tau_1^2}\cos(s_1\ell)H + G \\ 0 & -2\frac{s_1^2}{\tau_1^2}\cos(s_1\ell)N \end{bmatrix} \begin{bmatrix} B^a \\ \bar{B}_1^a \end{bmatrix} = \begin{bmatrix} iKM_{0m} - i\sum_{n=0}^{\infty} A_n\eta_n P_{nm} \\ iK\ell_{01} - i\sum_{n=0}^{\infty} A_n\eta_n V_{0n} \end{bmatrix}. \tag{4.103}$$

4.4 Numerical Results

This section presents a numerical analysis of the solution obtained for the anti-symmetric problem with a soft end at $z = 0$. The system is truncated using $n = 15$ terms, ensuring that the solution captures the key modes while maintaining computational efficiency. The analysis is conducted using the following parameter values: duct radius $a = 1\,\mathrm{cm}$, interface height $h = 1\,\mathrm{cm}$, viscosity coefficient $\mu = 1$, length $\ell = 0.5\,\mathrm{cm}$, speed of sound in air $c = 343.5\,\mathrm{m/s}$, and air density $\rho = 1.2$.

Figure 4.5 shows the real and imaginary parts of the pressure for the anti-symmetric problem as a function of the radius at $r = 0$ on the interface located at $z = -\ell$. It is observed that the real parts of the pressures in the regions $z < -\ell$ and $z > -\ell$ match exactly at the interface.

Similarly, the imaginary parts of the pressures in the regions $z < -\ell$ and $z > -\ell$ align precisely at the interface, which is consistent with the continuity condition of pressure. This consistency confirms the accuracy of the truncated solution and

validates the robustness of the numerical approach, even for the anti-symmetric configuration with a soft end at $z = 0$.

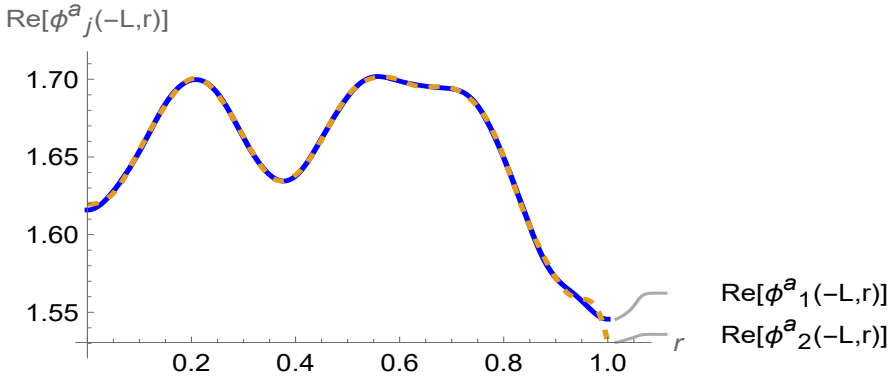

(a) Real parts

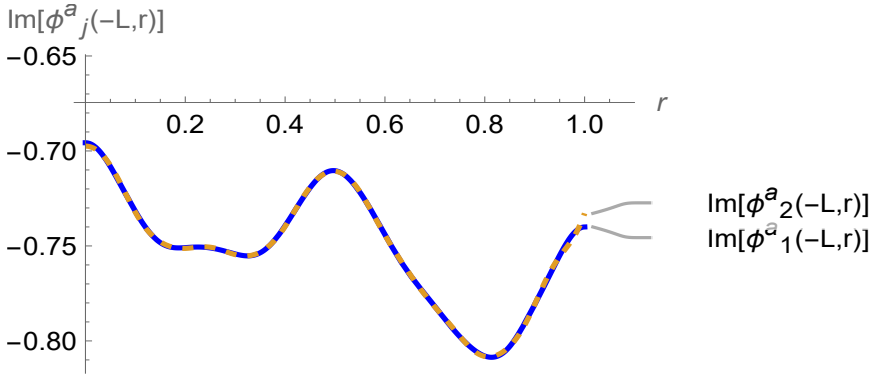

(b) Imaginary parts

FIGURE 4.5: With soft closed end: The real and imaginary parts of pressures versus radius r at interface $z = -\ell$, where $\mu = 1$, $\ell = 0.5$ and $a = 1$.

Figure 4.6 illustrates the real and imaginary parts of the normal velocity for the anti-symmetric problem as a function of the radius at $r = 0$ on the interface at $z = -\ell$.

It is clearly seen that the real parts of the normal velocity in the regions $z < -\ell$ and $z > -\ell$ coincide at the interface.

Likewise,

the imaginary parts of the normal velocity in these regions match exactly at the interface, which satisfies the continuity condition for normal velocity.

This agreement reinforces the accuracy of the truncated solution and highlights the effectiveness of the numerical method under the anti-symmetric configuration

with a soft end at $z = 0$.

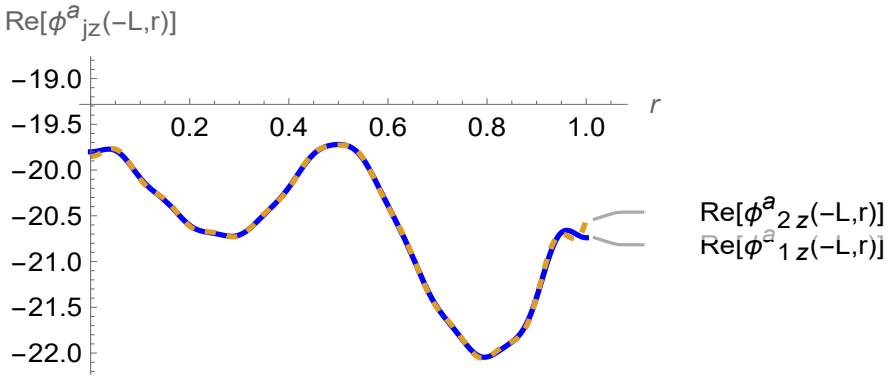

(a) Real parts

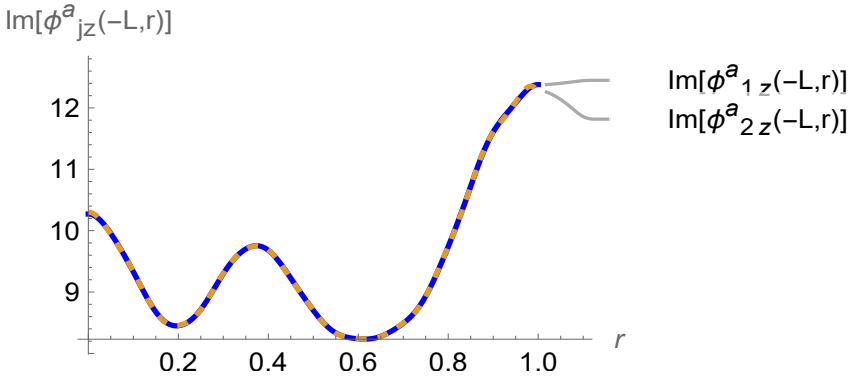

(b) Imaginary parts

FIGURE 4.6: With soft closed end: The real and imaginary parts of normal velocities versus radius r at interface $z = -\ell$, where $\mu = 1$, $\ell = 0.5$ and $a = 1$.

Chapter 5

Summary and Conclusion

The thesis thoroughly investigates modal behavior and exceptional points, delivering key insights into the impact of impedance conditions in waveguide systems. First acoustic wave propagation in an infinite waveguide, where the region at $z > 0$ is bounded by a general impedance condition is presented. The problem involves an EP_2 point, which introduces additional complexity in the wave behavior due to the coupling of modes at the exceptional point.

An extended mode-matching solution is employed to accurately resolve the problem by considering the continuity of both pressure and velocity at the interface. To confirm the performed algebra and computational efficiency, the system is truncated by considering a finite number of terms. The numerical results demonstrate that the solution converges effectively with the selected truncation, highlighting the accuracy of the method. The analysis shows that increasing the frequency leads to the excitation of higher-order modes, resulting in more intricate scattering patterns.

At lower frequencies, the scattering behavior is primarily dominated by the fundamental mode, resulting in relatively simple pressure and velocity distributions. However, as the frequency increases, the interaction between the incident wave and the duct geometry becomes more pronounced, causing the excitation of additional modes and the emergence of complex interference patterns.

In the following analysis, the propagation of waves through modes in a waveguide with both rigid and soft closed ends is investigated in detail. The extended mode-matching method is utilized to handle the general impedance conditions involving EP_2. This method enables a comprehensive analysis by accurately capturing the effects of both symmetric and anti-symmetric modes. The symmetric and anti-symmetric modes are determined using the mode-matching approach, where the continuity conditions at the interface are carefully enforced to ensure consistency across the boundaries. The application of an additional mode within the extended mode-matching framework allows for precise matching of the continuity conditions at both rigid and soft closed ends. This improvement enhances the accuracy and robustness of the numerical solution, ensuring that the computed results reflect the true physical behavior of the wave propagation in the waveguide. To solve the problem numerically, the solution is truncated after considering a sufficient number of modes to capture the essential physics of the system while maintaining computational efficiency. The pressures and velocity profiles at the interface are computed and plotted to visualize the wave behavior under the imposed boundary conditions. The agreement between the computed pressure and velocity profiles at the interface validates the truncated solution and confirms the accuracy of the algebraic formulation. The consistency of the results with the imposed boundary conditions and the smooth transition of the solutions across the interface further demonstrate the reliability of the extended mode-matching approach for analyzing wave propagation in complex waveguide structures.

Bibliography

[1] J. B. Lawrie, B. Nennig, and E. Perrey-Debain. Analytic mode-matching for accurate handling of exceptional points in a lined acoustic waveguide. *Proceedings of the Royal Society A*, 478(2268):20220484, 2022.

[2] D. John and S. Alice. Noise reduction via exceptional points in symmetric acoustic waveguides. *Journal of Applied Acoustics*, 150:123–135, 2025.

[3] B. J. Tester. The optimization of modal sound attenuation in ducts, in the absence of mean flow. *Journal of Sound and Vibration*, 27(4):477–513, 1973.

[4] L. Novotny and C. Hafner. Light propagation in a cylindrical waveguide with a complex, metallic, dielectric function. *Physical review E*, 50(5):4094, 1994.

[5] S. W. Rienstra. A classification of duct modes based on surface waves. *Wave Motion*, 37(2):119–135, 2003.

[6] E. J. Brambley and N. Peake. Classification of aeroacoustically relevant surface modes in cylindrical lined ducts. *Wave Motion*, 43(4):301–310, 2006.

[7] L. Laguerre F. Benmeddour, F. Treyssède. Numerical modeling of guided wave interaction with non-axisymmetric cracks in elastic cylinders. *International journal of Solids and Structures*, 48(5):764–774, 2011.

[8] E.-M. Graefe and H. F. Jones. Pt-symmetric sinusoidal optical lattices at the symmetry-breaking threshold. *Physical Review A*, 84(1):013818, 2011.

[9] W. Bi and V. Pagneux. New insights into mode behaviours in waveguides with impedance boundary conditions. *arXiv preprint arXiv:1511.05508*, 2015.

[10] F'elix, A. Maurel, and J.-F. Mercier. Improved multimodal methods for the acoustic propagation in waveguides with finite wall impedance. *Wave Motion*, 54:1–10, 2015.

[11] M. Afzal and H. Bilal. Acoustic wave scattering from a wavebearing cavity in a rectangular waveguide. *The Journal of the Acoustical Society of America*, 144(3 Supplement):1681, 2018.

[12] T. Goldzak, A. A. Mailybaev, and N. Moiseyev. Light stops at exceptional points. *Physical Review Letters*, 120:013901, 2018.

[13] M. Kelsten. *Modeling of acoustic waves in pipes with impedance walls and double roots*. PhD thesis, Rutgers University-School of Graduate Studies, 2018.

[14] M. Afzal and H. Bilal. Acoustic wave scattering from a wave-bearing cavity in a rectangular waveguide. *The Journal of the Acoustical Society of America*, 144(3_Supplement):1681–1681, 2018.

[15] A. Krasnok, D. Baranov, H. Li, M.-A. Miri, F. Monticone, and A. Al'u. Anomalies in light scattering. *Advances in Optics and Photonics*, 11:892–951, 2019.

[16] X. Qiu, L. Du, X. Jing, and X. Sun. The cremer concept for annular ducts for optimum sound attenuation. *Journal of Sound and Vibration*, 438:383–401, 2019.

[17] Z. Zhang, H. Bodén, and M. Åbom. The cremer impedance: An investigation of the low frequency behavior. *Journal of Sound and Vibration*, 459:114844, 2019.

[18] A. Krasnok, D. Baranov, H. Li, M. A. Miri, F. Monticone, and A. Alú. Anomalies in light scattering. *Advances in Optics and Photonics*, 11(4):892–951, 2019.

[19] M. A. Miri and A. Alu. Exceptional points in optics and photonics. *Science*, 363(6422):eaar7709, 2019.

[20] R. Kirby and W. Duan. Guided wave propagation in cylindrical ducts with elastic walls enclosing a fluid moving with a uniform velocity. *Wave Motion*, 85:1–9, 2019.

[21] M. Afzal, J. U. Satti, and R. Nawaz. Scattering characteristics of non-planar trifurcated waveguides. *Meccanica*, 55(5):977–988, 2020.

[22] Y. Ashida, Z. Gong, and M. Ueda. Non-hermitian physics. *Advances in Physics*, 69(3):249–435, 2020.

[23] W. Guo, J. Liu, W. Bi, D. Yang, Y. Aurégan, and V. Pagneux. Spatial transient behavior in waveguides with lossy impedance boundary conditions. *arXiv preprint arXiv:2010.03646*, 2020.

[24] M. Åbom and S. Jacob. A comment on the correct boundary conditions for the cremer impedance. *JASA Express Letters*, 1(2), 2021.

[25] M. Afzal, S. Shafique, and A. Wahab. Analysis of traveling waveform of flexible waveguides containing absorbent material along flanged junctions. *Communications in Nonlinear Science and Numerical Simulation*, 97:105737, 2021.

[26] E. J. Bergholtz, J. C. Budich, and F. K. Kunst. Exceptional topology of non-hermitian systems. *Reviews of Modern Physics*, 93(1):015005, 2021.

[27] M. A. Langthjem and M. Nakano. On the acoustic trapped modes and their symmetry properties in a circular cylindrical waveguide with a cavity. *Journal of Engineering Mathematics*, 128(1):14, 2021.

[28] M. Afzal, S. Shafique, and A. Wahab. Analysis of traveling waveform of flexible waveguides containing absorbent material along flanged junctions. *Communications in Nonlinear Science and Numerical Simulation*, 97:105737, 2021.

[29] M. Afzal, T. Nawaz, and R. Nawaz. Scattering characteristics of planar trifurcated waveguide structure containing multiple discontinuities. *Waves in Random and Complex Media*, 32(6):2776–2795, 2022.

[30] H. Afsar and M. M. Alam. Mode-matching analysis of flexural trifurcated waveguide with porosity effects. *Waves in Random and Complex Media*, pages 1–24, 2022.

[31] R. Kononchuk, J. Cai, F. Ellis, R. Thevamaran, and T. Kottos. Exceptional-point-based accelerometers with enhanced signal-to-noise ratio. *Nature*, 607(7920):697–702, 2022.

[32] R. Duggan, S. A. Mann, and A. Alu. Limitations of sensing at an exceptional point. *ACS Photonics*, 9(5):1554–1566, 2022.

[33] D. Li, Y. Gu, H. Ma, Y. Li, Ling Zhang, R. Li, R. Hao, and E-P. Li. Deep learning inverse analysis of higher order modes in monocone tem cell. *IEEE Transactions on Microwave Theory and Techniques*, 70(12):5332–5339, 2022.

[34] M. Farooqui, Y. Aurégan, and V. Pagneux. Ultrathin resistive sheets for broadband coherent absorption and symmetrization of acoustic waves. *Physical Review Applied*, 18(1):014007, 2022.

[35] B. Tiryakioglu and H. Ozturk. Mode-matching analysis for sound propagation in a cylindrical duct with a partial lining. *Acoustical Physics*, 69(4):436–441, 2023.

[36] A. D. Alruwaili, M. Afzal, H. N. Alahmadi, and A. Wahab. Wave scattering in cylindrical waveguides: Analyzing flexible shells and liner conditions. *Alexandria Engineering Journal*, 91:610–619, 2024.

[37] R. Nawaz, A. Yaseen, H. Alahmadi, and B. Tiryakioglu. A mode-matching analysis of flexible shells and waveguides with partitioning and muffler conditions. *International Journal of Mechanics and Materials in Design*, 20(5):1009–1028, 2024.

[38] J. Dai, D. Wang, Y. Fang, and Q. H. Liu. Efficient computation of electromagnetic waves under cylindrical geometries using spectral numerical mode matching (snmm) method. *IEEE Transactions on Antennas and Propagation*, 2024.

[39] H. Yang and W. Seong. Acoustic transmission loss of a cylindrical silencer filled with multilayer poroelastic materials based on mode-matching method. *Journal of Marine Science and Technology*, 2024.

[40] Y. Lu, D. Dong, X. Li, C. Hu, M. Wang, C. Chen, Y. Liu, H. Ji, and Y. Fu. Acoustic rainbow trapping in cylindrical spoof waveguide. *Applied Acoustics*, 231:110502, 2025.

[41] L. E. Kinsler, A. R. Frey, A. B. Coppens, and J. V. Sanders. *Fundamentals of acoustics*. John Wiley & Sons, 2000.

[42] G. G. Stokes. On the theories of the internal friction of fluids in motion, and of the equilibrium and motion of elastic solids. *Fluids*, 2007.

[43] S. S. Rao. *Vibration of continuous systems*. John Wiley & Sons, 2019.

[44] F. Mir and S. Banerjee. Performance of a multifunctional spiral shaped acoustic metamaterial with synchronized low-frequency noise filtering and energy harvesting capability. In *Smart Materials, Adaptive Structures and Intelligent Systems*, volume 84027, page V001T01A006. American Society of Mechanical Engineers, 2020.